energies

MDPI

Article

Feasibility Study of Fluctuating Wind Pressure around High-Rise Buildings as a Potential Energy-Harvesting Source

Jae-Chan Park, In-Ho Kim and Hyung-Jo Jung *

Department of Civil and Environmental Engineering, Korea Advanced Institute of Science and Technology, 291 Daehak-ro, Yuseong-gu, Daejeon 34141, Korea; wocks1226@kaist.ac.kr (J.-C.P.); kih119@kaist.ac.kr (I.-H.K.)
* Correspondence: hjung@kaist.ac.kr

Received: 29 July 2019; Accepted: 21 October 2019; Published: 23 October 2019

Abstract: As the importance of sustainable energy increases, wind power generation systems utilizing wind energy around high-rise buildings are being developed. However, in existing wind turbine systems, it is necessary to solve noise, vibration problems, and structural issues for the installation of large-sized systems. In addition, small wind turbine systems can be installed only in limited areas such as roofs and corners, because their efficiency is limited to high and stable wind speed. For this reason, the distribution of fluctuating wind pressure around high-rise buildings was analyzed, and its feasibility as an energy source was evaluated, reflecting that fluctuating wind pressure can be used in vibration-based energy-harvesters. To achieve this, firstly, experimental conditions and theories were established to check the characteristic of wind pressure around high-rise buildings. The experiment was divided into the environment without surrounding buildings and the urban environment. Next, the pressure distribution around high-rise buildings and the quantitative results obtained from the experiment were determined. Finally, based on the results obtained from the experiments, the feasibility of fluctuating wind pressure as an energy-harvesting source was analyzed. From this study, it was found that fluctuating wind pressure can be used as a new energy source at new locations of high-rise buildings that were not utilized previously.

Keywords: high-rise building; fluctuating wind pressure; static wind pressure; energy-harvesting source; wind tunnel test

1. Introduction

Wind power receives great attention as a renewable energy source. Because wind power is eco-friendly and sustainable for the production of electric energy, it receives great social acceptance [1]. Therefore, its utilization increased in recent years. According to the five-year forecast following almost 60 GW of new wind power installations in 2017, an annual market of 75 GW is expected by 2021, and an accumulated capacity of more than 800 GW is expected by the end of 2021 [2]. In general, most wind power generation systems are located in areas affected by wind, such as hills and coasts. However, their importance in urban environments is increasing. The research and development of building-integrated wind turbine (BIWT) systems is actively being pursued in accordance with such situations. Currently, Europe, the United States, and China, which have policies for eco-friendly carbon reduction, are leading research on BIWT systems [3].

Wind Energy for the Built Environment (WEB) (2001) proposed that large-scale wind power generation systems can be applied to high-rise buildings with an aerodynamic shape [4]. Seven optimal building forms were selected through computational fluid dynamics (CFD) and wind tunnel experiments. The system installed between twin towers provided considerable efficiency compared

with other systems. The Bahrain World Trade Center was the first building with large wind turbines. The two buildings support three 29-m-diameter horizontal-axis wind turbine (HAWT) systems. Smith et al. (2007) informed that the amount of energy using the integrated BIWT systems was almost 1100–1300 MWh per year [5]. This result was 11–15% of the total consumed energy of the building. The Bahrain World Trade Center is shown in Figure 1a. Pearl River Tower was designed to be a zero-energy building [6]. This building has two open spaces between three parts of the building. Eight 5-m-diameter Darrieus wind turbines are set up in the area of open space. Pearl River Tower is shown in Figure 1b. Strata Tower is a new 43-storey, 148-m-tall tower designed for sustainable regeneration [7]. This tower has three HAWT systems at the top of the building, and the diameter of their rotors is 9 m. Strata Tower is shown in Figure 1c. Although these systems have the advantage of producing large-scale electricity, they have drawbacks such as the need to consider noise, vibration problems, and structural factors due to their large size. In order to install large-scale BIWT systems in high-rise buildings, the structural issues have to be considered in the design process.

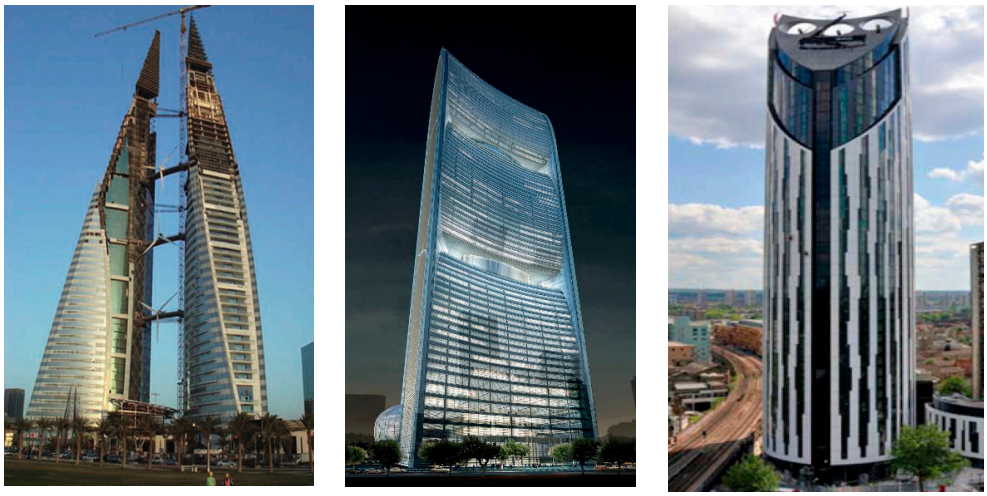

(**a**) (**b**) (**c**)

Figure 1. Large-scale building-integrated wind turbine (BIWT) systems: (**a**) Bahrain World Trade Center [5]; (**b**) Pearl River Tower [6]; (**c**) Strata Tower [7].

Small-scale wind turbines are used as a convenient and widespread technology to redeem the limitations of large-scale BIWT systems. In the small-scaled system, vertical axis wind turbines (VAWTs) are used more than HAWTs because VAWTs utilize drag force in a limited area, compared to HAWTs which utilize lift force [8]. Moreover, VAWTs are able to easily generate electric power under low wind speeds in urban space. Typical types of small-scale wind turbine systems are shown in Figure 2. In previous studies on small-scale wind power systems, McTavish et al. (2011) developed an assessment of the efficiency of a novel VAWT using CFD analysis [9]. Abdalrahman et al. (2017) suggested smart control technologies on the basis of a neural network access for creating an individual blade pitch control system of an H-type VAWT system for improving its power generation performance [10]. Jin et al. (2018) indicated that the efficiency of VAWTs can be improved by properly selecting parameters of the turbine [11]. Furthermore, studies on the application of VAWTs surrounding high-rise buildings were conducted. Sharpe et al. (2010) proposed Crossflex wind turbines [12]. The Crossflex proposal was an innovative developed type of a Darrieus turbine form. This turbine was designed as a module that can be located on ridges and corners of high-rise buildings to generate meaningful levels of power. Chong et al. (2012) researched a new type of VAWT for high-rise buildings [13]. The omni-directional guide vane (ODGV), which uses VAWTs, was proposed to increase the rotor performance. Considering previous studies, the installation area for small wind turbines is mainly limited to rooftops and corners where wind speed is fast and stable.

(**a**) (**b**) (**c**)

Figure 2. Small-scale wind turbine systems: (**a**) horizontal-axis wind turbine (HAWT) system [8]; (**b**) vertical-axis wind turbine (VAWT) system, H-type [14]; (**c**) Crossflex wind turbine system [12].

To overcome this limitation, various studies were conducted to utilize the wind energy generated around the outer walls of high-rise buildings. Bayoumi et al. (2013) analyzed the distribution of wind velocity on the exterior wall of high-rise buildings and discussed the applicability of VAWTs [15]. This method could be used in the early process of design when installing VAWTs around a high-rise building. Park et al. (2015) devised a new type of BIWT system [16]. The system consists of a guide vane that collects and increases wind velocity, and an appropriate rotor for the conditions of high-rise buildings. Hassanli et al. (2017) suggested a double-skin façade (DSF) system. The system deals with strategic openings for harvesting wind energy around high-rise buildings [17]. The DSF was designed to increase the flow in the cavity for an incident angle of wind. From the above studies, energy can be obtained by installing a small turbine on the outer wall of a high-rise building. However, there is a disadvantage, whereby it cannot be used in a wide area on the surface of a building. Therefore, wind power turbines used in high-rise buildings can obtain limited electrical energy due to the limited space of the installation site. For this reason, a new type of wind energy source is necessary for obtaining additional electric energy, outside of the area where conventional wind power turbine systems used in high-rise buildings are installed.

In this study, fluctuating wind pressure that causes vibrational energy around high-rise buildings was analyzed, reflecting the studies on energy-harvesting devices that convert vibration energy into electric energy. The fluctuating wind pressure creates vibrational energy unlike the constant wind speed necessary for conventional wind turbine systems. Therefore, it is expected that additional energy can be obtained through fluctuating wind pressure in areas other than roofs or corners of high-rise buildings where conventional wind turbine systems are installed.

Recently, studies were conducted to identify wind pressure distribution around high-rise buildings using CFD [18]. Zhao et al. (2017) studied the effects of architectural shapes on surface wind pressure distribution [19]. For the study, a specific case was analyzed (oval-shaped tall buildings). However, because of the fluctuating wind components from complex turbulence components of the approaching flow, an accurate prediction of fluctuating wind pressure characteristics using numerical analysis is difficult. For this reason, in this study, the wind pressure distribution around high-rise buildings was analyzed using a wind tunnel experiment.

To achieve this, firstly, the conditions and theories related to the experiment for analyzing the fluctuating wind pressure formed around high-rise buildings were explained. This study analyzed wind pressure around high-rise buildings without considering the effect of surrounding buildings and similarly sized buildings in the urban environment. For the analysis, the distribution of static and fluctuating wind pressure around high-rise buildings and the quantitative results obtained from the experiment were discussed to comprehensively understand the characteristics of the fluctuating wind

pressure as an energy-harvesting source. Finally, the feasibility of fluctuating wind pressure around high-rise buildings as an energy-harvesting source was evaluated. For the evaluation, an analytical model of the vibration based on a simple energy-harvesting device using fluctuating wind pressure as an excitation force was utilized. Unlike previous research, this study evaluated the feasibility of a new type of energy source that was not previously utilized around high-rise buildings. The results of this study can be used for the development of new types of energy-harvesting devices that can be installed in locations different from conventional wind turbine systems used around high-rise buildings.

2. Experimental Study of Wind Pressure Around High-Rise Buildings

In this section, the wind pressure distribution around high-rise buildings was analyzed using a wind tunnel experiment. The distribution of wind pressure around high-rise buildings is different from wind speed distribution due to various factors. Also, there are various distributions depending on the type of pressure. This study analyzed the distribution of static pressure and fluctuating wind pressure around high-rise buildings to comprehensively understand the characteristics of fluctuating wind pressure as an energy source. However, an accurate prediction of fluctuating wind pressure characteristics using numerical analysis is extremely difficult due to he fluctuating wind components from the complex turbulence components of approaching flow [20]. Elements that determine fluctuating wind pressure generated around high-rise buildings in the boundary layer vary, such as turbulence of the wind blowing and vortex shading, and the wake caused by turbulent separation. Therefore, an exact theoretical principle of fluctuating wind pressure caused by vortex flow and wake flow is yet to be discovered [20]. For these reasons, in this study, wind pressure distribution was investigated using a wind tunnel experiment.

2.1. Experimental Setting

The conditions and theories for the experimental setting are described below. The high-rise buildings for the experiment had a longitudinal length, lateral length, and height of 45 m, 25 m, and 180 m, respectively. The wind environment around the high-rise buildings were analyzed using a miniature model reduced in scale by 1:500; therefore, the size of the reduced high-rise building model was $90 \times 50 \times 360$ mm^3 (i.e., longitudinal length × lateral length × height). There were 364 wind pressure-measuring taps in total. There were 117 pressure taps and 65 pressure taps on each side. Figure 3 shows the model size and distribution of the pressure taps.

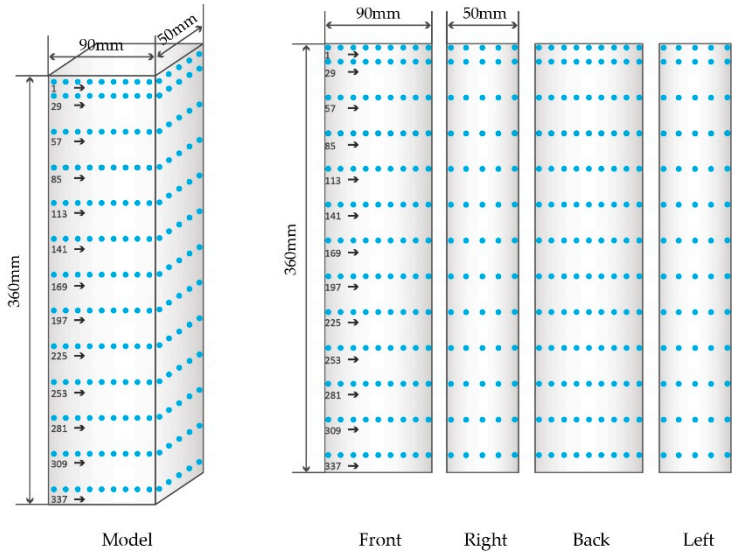

Figure 3. Model size and distribution of pressure taps.

The pressure taps were connected to six 64-connection pressure scanners from Scanivalve Corp. (model: ZOC 33/64Px) [21]. The electronic pressure-scanning module converts them to high-level electronic signals. This system is a globally proven equipment for wind tunnel experiments in the construction, civil, and aerospace fields [22–25]. This electronic pressure-scanning module can accurately measure unsteady pressure signals within a small margin of error. A brief summary of the specifications of ZOC 33/64Px is shown in Table 1.

Table 1. Specification of ZOC 33/64Px for the wind tunnel test [21].

Inputs (Px)	Full Scale Ranges	Accuracy	Full Scale Output	Scan Rate
64Px, 1.067 mm outer diameter tubulation	±2.5, ±5, ±7, ±17, ±35, ±100, ±350 kPa	7 kPa: ±0.12% full scale 15 kPa: ±0.10% full scale 35 to 350 kPa: ±0.08% full scale	Standard: ±2.5 Vdc Optional: ±5 Vdc, ±10 Vdc	45 kHz

When the wind blows from the high level of the atmospheric layer to the ground at a constant wind speed, frictional force is generated by the roughness of the ground surface and the viscosity of the air [18]. As a result, the wind speed on the ground decreases, which causes turbulent motion [18]. The wind constantly blowing in the upper part of the atmosphere decreases in speed and accompanies the turbulence movement because of the frictional force [26]. The gradient wind layer is the layer from a height of 300 m to 600 m above the ground. The wind in this layer exhibits laminar flow with little change in speed. The boundary layer is the region existing between the gradient wind layer and the ground surface. The wind speed at the boundary layer changes according to the height. The vertical distribution of the wind speed of the boundary layer is described by the exponential power law and the logarithm law [27,28]. Considering the atmospheric boundary layer theory, this study used the exponential power law for the vertical distribution of the wind speed. The exponential power law is shown below.

$$\frac{U}{U_H} = \left(\frac{Z}{Z_H}\right)^a. \quad (1)$$

In Equation (1), U is the wind speed at height Z, Z_H is the reference height, U_H is the wind speed at the reference height, and a is the vertical wind profile exponent [27]. In the case of the exponential power law, it is used at a height of 100 m above the ground surface [27]. For the analysis, the reference speed blown in a high-rise building with a height of 180 m was selected as 40 m/s, which was used as the designed wind speed of the building. The scale of the wind speed was set to 1/6. Therefore, the wind speed for the experiment was set at 6.67 m/s. Because the vertical wind profile exponent is distinguished by the characteristics of the terrain, the characteristics of strong winds are mainly determined by the condition of the surface for the wind [29]. Therefore, it is necessary to reproduce the state of the surface for the wind that actually blows in the wind tunnel. However, it is not easy to change the state of the wind tunnel floor for each case because it requires substantial experimental cost and time. For this reason, the standard vertical wind profile exponent was used for the experiment [29]. The criteria of the vertical wind profile exponent were introduced in codes IEC 61400-3, American Society of Civil Engineers (ASCE 7-10), National Building Code of Canada (NBCC 2010), and Architectural Institute of Japan (AIJ 2004). In this study, reflecting the criteria of ASCE 7-10 and the topographical characteristics of Seoul, Republic of Korea, the vertical wind profile exponent was chosen as 0.25%.

Walls, spires, and blocks were placed in a wind tunnel with a width of 8 m, a height of 2.5 m, and a length of 23.2 m in order to reproduce the 0.25% vertical wind profile exponent. In the case of the blocks for the vertical wind profile exponent, two types of blocks were arranged in the wind tunnel (A type: $100 \times 100 \times 100$ mm^3; B type: $50 \times 50 \times 50$ mm^3). In order to obtain results for various angles

of wind attack, a base that can be rotated was installed under the model. Figure 4 gives the schematic of the wind tunnel.

Figure 5 gives the vertical distribution of the wind speed and turbulence intensity obtained from the measured results through an anemometer, and the theoretical results from the exponential law. The wind speed was measured up to a height of 1 m at 22 intervals using the anemometer. The experimental results showed that the conditions of the wind tunnel were appropriate for the main experiment.

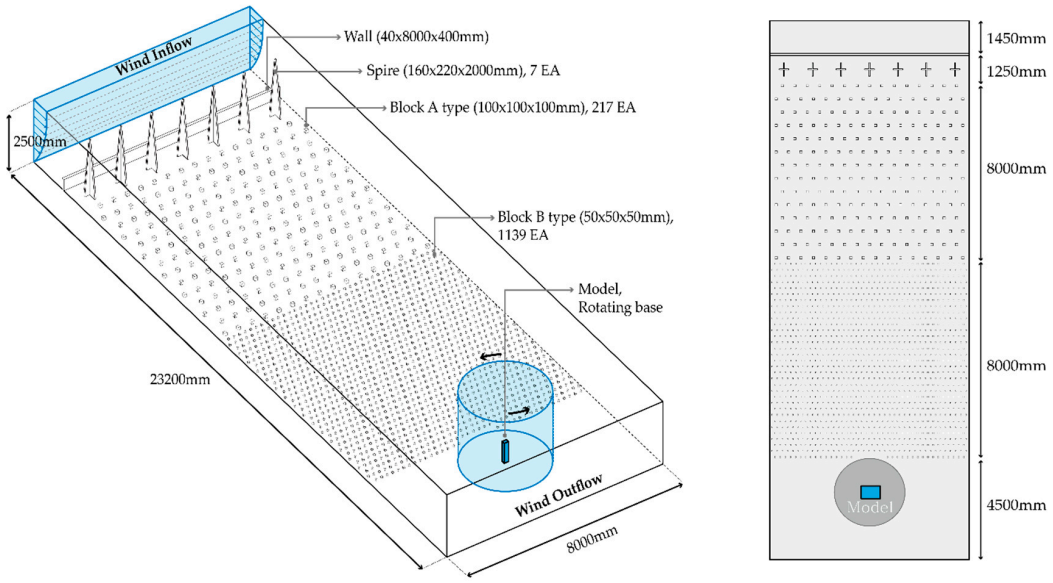

(**a**) (**b**)

Figure 4. Schematic of the wind tunnel: (**a**) outline; (**b**) upper view.

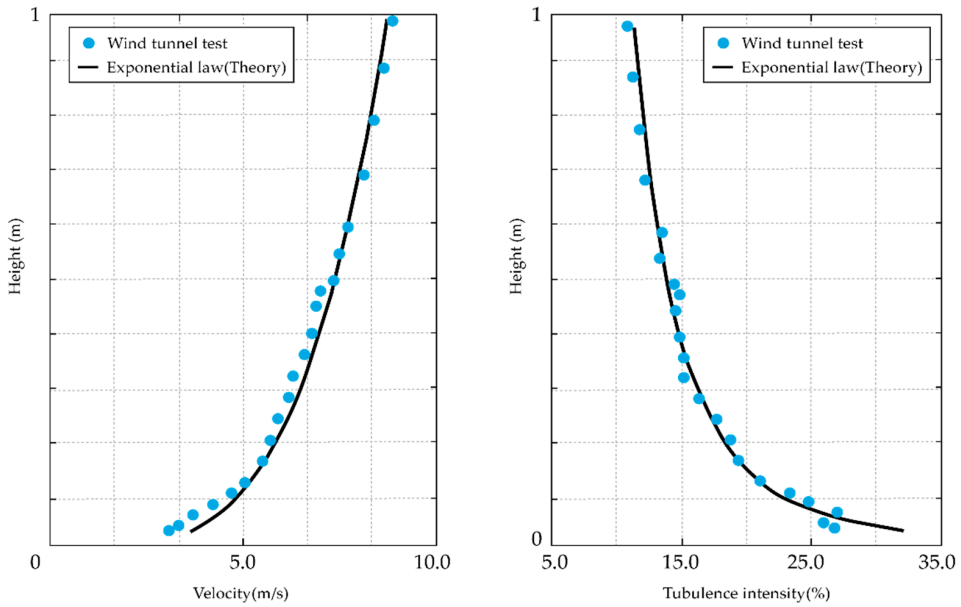

(**a**) (**b**)

Figure 5. Vertical distribution of the wind speed and turbulence intensity: (**a**) vertical distribution of wind speed; (**b**) vertical distribution of turbulence intensity.

The experiment analyzed the distribution of wind pressure in a high-rise building without surrounding buildings and a high-rise building in the urban environment. For the building without surrounding buildings, the wind pressure was measured through the angles of wind attack from 0° to 90° with increments of 30°. An angle of wind attack of 0° means that the wind is blowing perpendicular to the front surface of the building. Conditions of the experiment for the high-rise building without surrounding buildings are shown in Figure 6. In the case of the building in the urban environment, the site was designated as Seoul in Korea. A 12–16-m-tall building was located toward the front of the site. A 20-m-high building was located on the left side of the site. Finally, 154-m-high and 172-m-high buildings were located on the right side of the site. Hence, it was possible to check the influence of surrounding buildings at various heights. The distribution of wind pressure around a high-rise building depends on the height, shape, and arrangement of the surrounding buildings. It is impossible to define the absolute wind pressure distribution around high-rise buildings under the influence of neighboring buildings. Therefore, the results of this study were checked to analyze the effect of surrounding buildings on the wind pressure distribution of the high-rise building. The wind pressure was measured through a range of angles of wind attack from 0° to 360°. Conditions of the urban building experiment are shown in Figure 7.

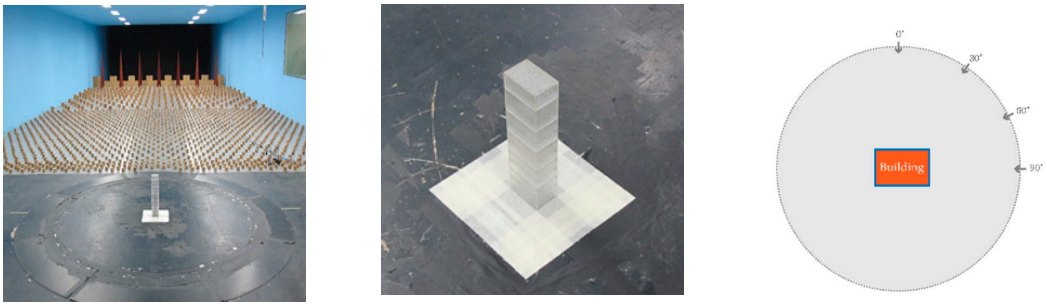

(**a**) (**b**) (**c**)

Figure 6. Conditions of the experiment (without surrounding buildings): (**a**) setting of the experiment; (**b**) the model of the experiment; (**c**) schematic of the angles of wind attack.

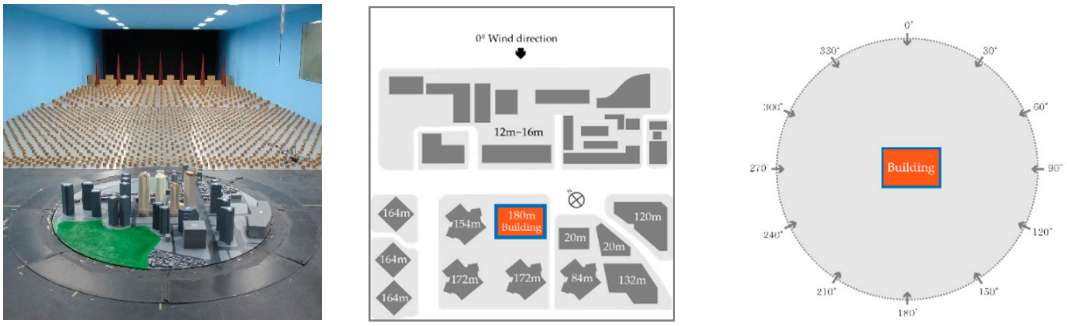

(**a**) (**b**) (**c**)

Figure 7. Conditions of the experiment (the urban environment): (**a**) setting of the experiment; (**b**) schematic of building layout; (**c**) schematic of the angles of wind attack.

In both experiments, the wind speed blown onto the high-rise building at the actual scale was set to 40 m/s, the scale of the wind speed was set to 1/6, and the wind speed in the wind tunnel was set to 6.67 m/s. The similarity law was used to apply the wind tunnel experiments to the actual scale [30]. The similarity law is shown in Equation (2). The time scale ($T_{model}/T_{full-scale}$) becomes 1/83.33 according to Equation (2) for the ratio of the model scale to the full-size building ($L_{model}/L_{full-scale}$) and the ratio of

the model scale to the full-size wind speed (V_{model}, $V_{full-scale}$). Sampling frequency for the wind tunnel test was 625 Hz. Based on this, 50,000 data points for 80 s were obtained and analyzed through the experiment. The time measured through the experiment was about 6666 s at the full scale.

$$\frac{T_{model}}{T_{full-scale}} = \frac{L_{model}}{L_{full-scale}} / \frac{V_{model}}{V_{full-scale}}. \quad (2)$$

2.2. Experimental Results

In this section, in order to analyze wind pressure distribution around the high-rise building, the pressure coefficient was calculated. The wind pressure coefficient of pressure points on the building skin was calculated as follows:

$$C_{Pi}(t) = \frac{P_i(t) - P_\infty}{\rho U_H^2/2}, \quad (3)$$

where $C_{Pi}(t)$ is the wind pressure coefficient of the point, $P_i(t)$ is the local pressure acting on the point, P_∞ is the static pressure upstream of the tower, which is the reference pressure used to calculate the pressure coefficient, ρ is the density of air, and U_H is the reference velocity upstream of the tower at the reference height [31]. By calculating $C_{Pi}(t)$, the mean wind pressure coefficient $C_{pi,\ mean}$ and fluctuating wind pressure coefficient $C_{pi,\ rms}$ could be obtained as follows:

$$C_{pi,\ mean} = \frac{1}{N}\sum_{i=1}^{N} C_{pi}(t), \quad (4)$$

$$C_{pi,\ rms} = \sqrt{\frac{1}{N-1}\sum_{i=1}^{N}\left(C_{pi}(t) - C_{pi,\ mean}\right)}, \quad (5)$$

where N is the number of time samples [31]. The distributions of wind pressure around the high-rise building without surrounding buildings and the high-rise building in the urban environment affected by surrounding buildings were analyzed using the wind pressure coefficients.

2.2.1. Experimental Results for the High-Rise Building without Surrounding Buildings

Using the wind tunnel experiments, static and fluctuating wind pressure distributions generated by an angle of wind attack of 0° around the building were analyzed. The results are shown in Figures 8 and 9. Experimental results were checked by assigning numbers 1–4 to each building vertex (front: side 1–2, sides: sides 2–3, 4–1, back: side 3–4). In the case of the distribution of the mean wind pressure coefficient, a high positive value was shown at the center of the upper part (0.82 H) of side 1–2. The vicinity of this part is called a stagnation point. In fluid dynamics, the stagnation point is a point in a flow field where the local velocity of the fluid is zero [32]. The Bernoulli equation proves that the static pressure is the highest when the velocity is zero. Hence, the static pressure is at its maximum value at stagnation points [32,33]. The wind pressure generated on side 1–2 showed mainly positive pressure. Overall, the highest negative pressure occurred on the sides 2–3, 4–1. This is due to deconfliction occurring at the front corner. On side 4–1, negative pressure occurred due to deconfliction from the side edge, as well as the side face.

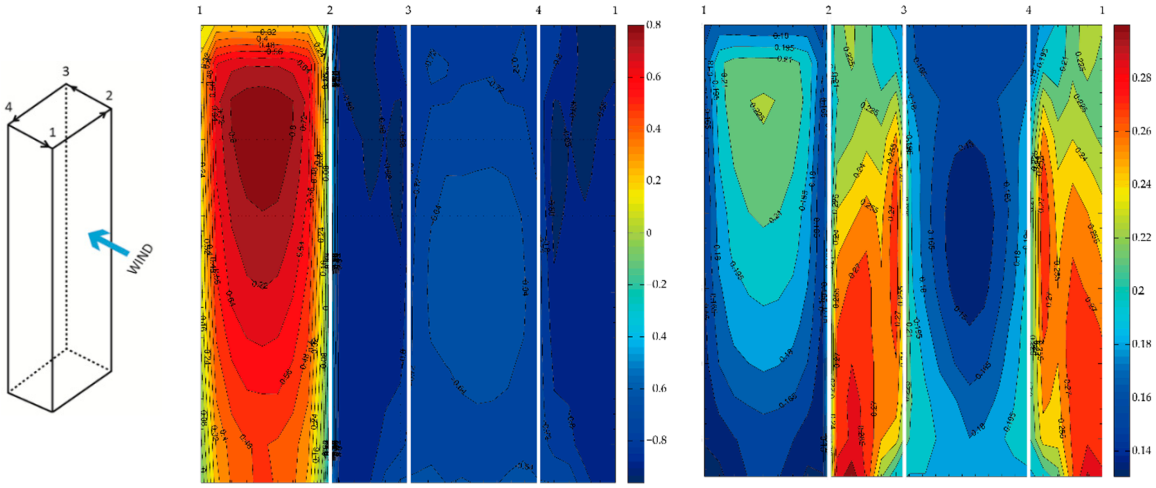

Figure 8. Wind pressure distribution around the high-rise building without surrounding buildings (0°): (**a**) mean wind pressure coefficient; (**b**) fluctuating wind pressure coefficient.

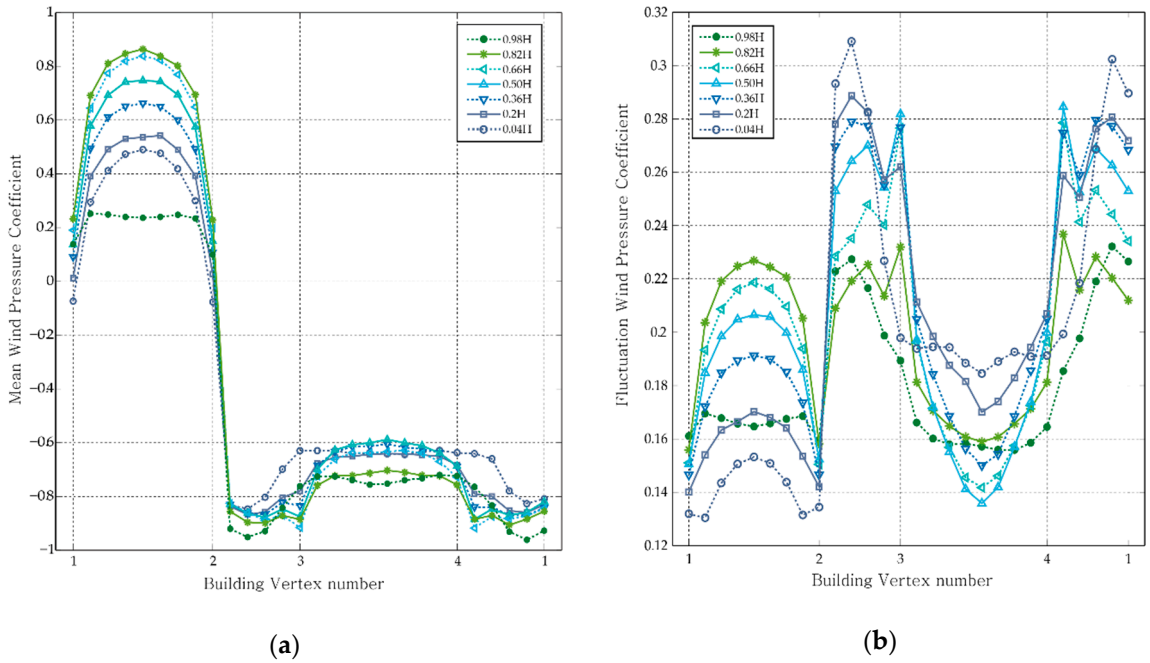

Figure 9. Wind pressure coefficient around the high-rise building without surrounding buildings (0°): (**a**) mean wind pressure coefficient; (**b**) fluctuating wind pressure coefficient.

In the case of fluctuating wind pressure coefficient, the pressure distribution was different from the mean pressure value. When wind blows on a tall building, deconfliction occurs at a height with time lag. As a result, a wind shear layer begins to be generated (Figure 10a). At this time, a vortex component is generated and moves to the lower part of the side surface [34]. This components gradually grow at the bottom of the building and form an inverted conical vortex (Figure 10c–e) [34]. Due to the vortex that grows downward, the turbulence intensity in the lower layer is larger. Because large turbulent intensity promotes vortex formation, high fluctuating wind pressure is generated on the side's lower layer. When the vortex has a certain level of energy, it is released to the back side (Figure 10f).

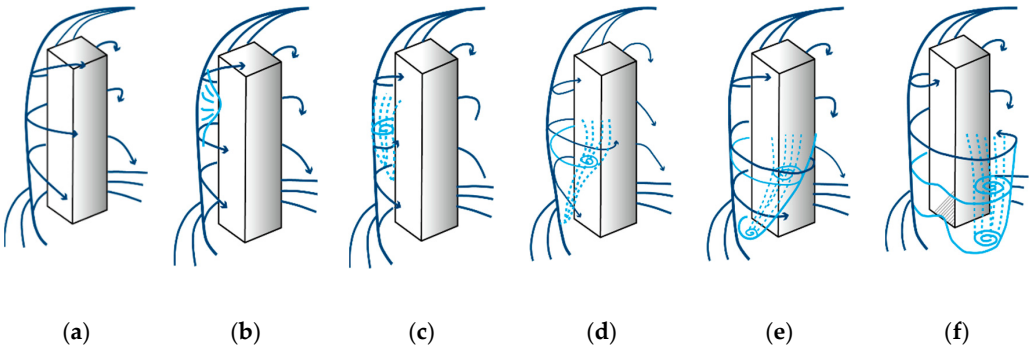

Figure 10. The process of formation and release of vortex shedding around a high-rise building [34]: (**a**) wind shear layer; (**b**) formation and movement of a vortex component; (**c**–**f**) formation and movement of an inverted conical vortex.

From the above procedure, the highest fluctuating wind pressure coefficient was shown in the lower part of sides 2–3, 4–1. On side 1–2, the upper part (0.82 H) showed a relatively high value. In the case of fluctuating wind pressure on side 3–4, as the vortex generated on sides 2–3, 4–1 was released to side 3–4, the lower part showed a relatively high value. From the results of the experiment, it was estimated that energy can be obtained from the middle and lower parts of the building by using vibration from fluctuating wind pressure, in addition to the upper part and corner of the building where high wind velocity can be obtained. In this study, it was judged that the vibration component with high negative pressure existing in the middle and lower parts of the side of a high-rise building is worthy of use as a new energy source.

Because of the above facts, the value (Pa) of the fluctuating wind pressure around the high-rise building was investigated. The values of the pressure were checked at the positions where the maximum fluctuating wind pressure coefficient (point 347) and minimum fluctuating wind pressure coefficient (point 338) were identified. Since the pressure data were obtained based on the designed wind speed for the experiment (40 m/s), it was necessary to change the wind speed. The reference wind speed was based on the average wind speed in Seoul, Republic of Korea. For the wind speed data, the annual average wind speed measured from 2011 to 2017 by the Korea Meteorological Administration was used. Because the data were measured from 10 m above the ground, the wind speed was changed by using the exponential power law for the reference speed. The average wind speed measured from 10 m above the ground was 2.67 m/s, and the reference wind speed for checking the pressure values was 5.49 m/s. Average annual wind speed data in Seoul are shown in Figure 11. The points of the maximum and minimum values of the fluctuating wind pressure coefficient are shown in Figure 12a. In the case of the pressure identified at point 338, it was primarily positive, and, in the case of the pressure identified at point 347, it was primarily negative. Time series data of wind pressure of these two points are shown in Figure 12b.

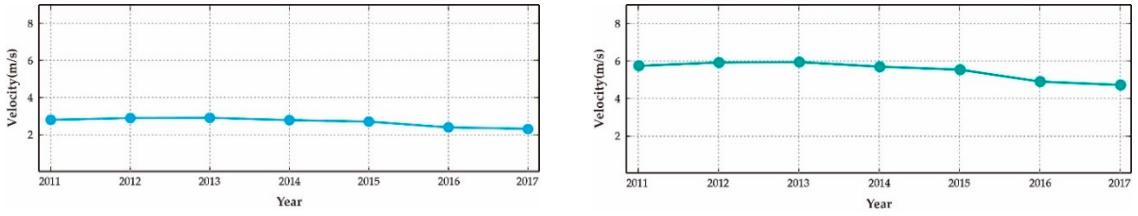

Figure 11. Wind speed data by year (Seoul, Republic of Korea): (**a**) average wind speed by year measured from 10 m above ground; (**b**) average wind speed by year measured from 180 m above ground (the reference speed for checking the pressure values around the high-rise building).

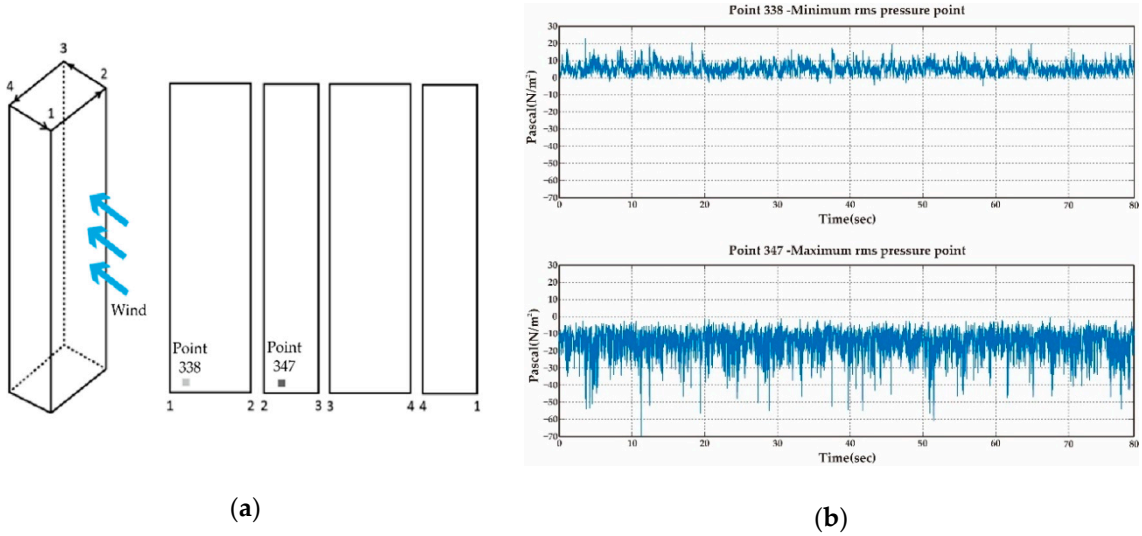

(**a**) (**b**)

Figure 12. The points with maximum and minimum root-mean-square (RMS) values of fluctuating wind pressure (without surrounding buildings): (**a**) the locations of the two points; (**b**) pressure data of each point.

Table 2 shows the pressure values of the points with maximum and minimum fluctuating coefficients. The unit of pressure described above is Pascal (N/m^2). At point 338, the maximum value was 22.94 Pa, the minimum value was −4.68 Pa, and the RMS value was 6.25 Pa. At point 347, the maximum value was −0.5522 Pa, the minimum value was −69.3 Pa, and the RMS value was 17.33 Pa. As a result, it was confirmed that the vibration corresponding to a maximum amplitude of 17.33 Pa was generated when a wind of 5.49 m/s was blown onto a high-rise building. It is expected that this value will be even higher in windier cities than Seoul.

Table 2. The pressure values at the points with the maximum and minimum root-mean-square (RMS) values of fluctuating wind pressure (without surrounding buildings).

Pressure Point	Max Value (Pa)	Min Value (Pa)	RMS Value (Pa)
Point 338 (minimum)	22.94	−4.68	6.25
Point 347 (maximum)	−0.55	−69.31	17.33

Wind pressure measurement results generated by wind blowing at various angles of attack (30°, 60°, and 90°) onto the high-rise buildings without surrounding buildings using the above method are shown in Appendix A. As per the results of measurement shown in the case of mean pressure coefficient, there were changes depending on the angle of attack. However, high pressure was mostly measured around the stagnation point on the upper part of the building. It is expected that energy using static pressure would be obtained in the upper part of the building (0.8 H).

In the case of fluctuating pressure coefficient, the distribution was different according to the angle of attack. When the wind flew at angles of attack of 30° and 60° on the tall building, it showed the highest energy at medium height in the form of narrow width. When the wind blew onto the high-rise building at an angle of attack of 0°, it showed high fluctuation due to deconfliction that occurred as it flowed onto the corners. However, in the case of the wind blowing at 30° or 60°, because the wind flew directly onto the angular corners, deconfliction was reduced. For this reason, the low part of the building side had a relatively small pressure compared to the case where it was affected by winds at an angle of attack of 0° when the wind was blown at an angle of attack of 30° or 60° onto the single high-rise building. For the angle of wind attack of 90°, it was similar to the fluctuating wind pressure pattern caused by the angle of wind attack of 0°. Based on the side 4–1 tangential to the wind attack, high values of fluctuating wind pressure coefficients were observed in the wide area of the lower parts

of sides 1–2, 3–4. Therefore, it was found that the influence of the wind angle on the fluctuating wind pressure distribution is very large. This is due to the pattern of deconfliction that occurs at the corners of the front edge, which changes with the angle of wind attack.

Finally, the frequency of fluctuating wind pressure around the high-rise building was analyzed. Generally, the frequency spectrum of fluctuating wind pressure of high-rise buildings is mainly expressed by dimensionless coefficients in wind engineering literature [35]. However, in this study, the frequency spectrum is expressed in hertz to analyze the frequency characteristics of wind pressure for energy-harvesting purposes. The frequency around the high-rise building was analyzed by selecting nine points at the same height. Also, the height was divided into four cases (0.02 H, 0.36 H, 0.62 H, and 0.98 H). The results of the frequency analysis of the nine points for each height are shown in Figure 13.

In the case of the low part of the building (0.02 H), the highest power density among the four cases was shown. In the case of fluctuating wind pressure occurring around side 1–2, a relatively high power density was mainly shown at frequencies between 1.5 and 3.5 Hz. In the case of side 2–3, the highest power density was measured on the three measured sides. The highest power density was shown to be between 5 and 7.5 Hz. In the case of side 3–4, most of the vibration components had a frequency range between 1.5 and 7.5 Hz. This is in agreement with the result of analyzing the distribution of the fluctuating wind pressure coefficient. In the case of the middle part of the building (0.35 H, 0.62 H), similar patterns to the low part were shown. It was shown that the vibration component became weaker as the height increased. In the case of the high part of the building (0.98 H), the pattern was different from the fluctuating wind pressure generated in the lower and middle parts. Overall, the vibration components at frequencies between 1.5 and 3.5 Hz were dominant. The weakest power density among the four cases was observed. As a result of analyzing all four cases, the vibration components at frequencies between 3 and 15 Hz were found to be dominant. Additionally, the frequency of the fluctuating wind pressure formed by the wind blowing at angles of attack from 30° to 90° was analyzed. However, because the overall range of frequency was similar to the case considering the angle of wind attack of 0°, the results of other cases (from 30° to 90°) were omitted.

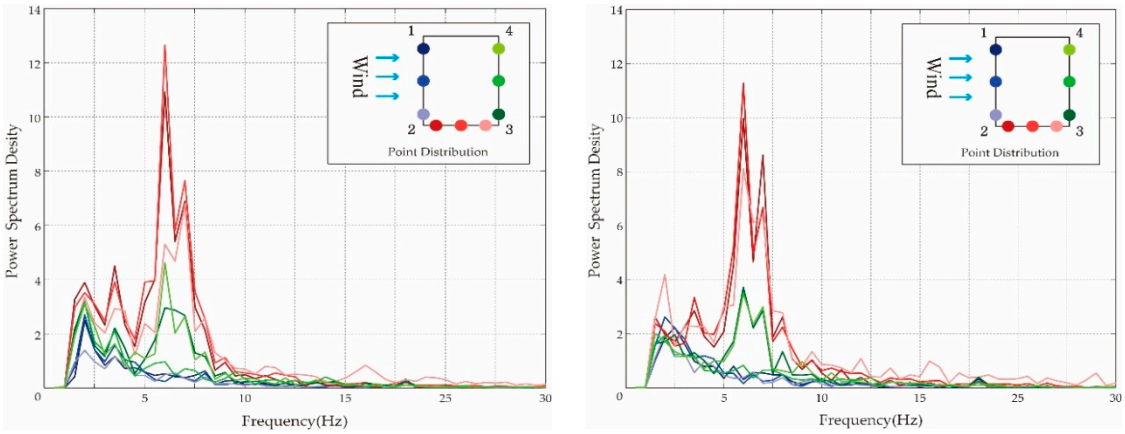

Figure 13. *Cont.*

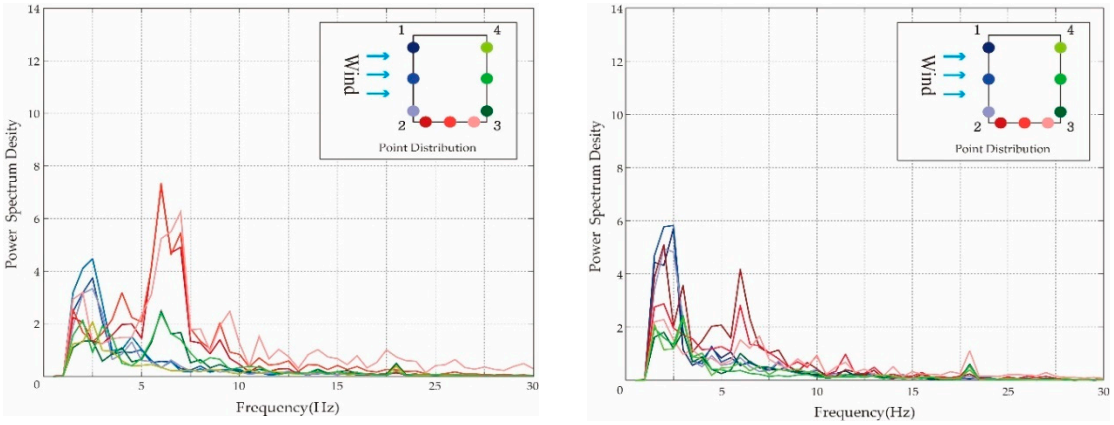

Figure 13. Frequency spectrum of wind pressure by height and location of the high-rise building without surrounding buildings: (**a**) 0.02 H; (**b**) 0.36 H; (**c**) 0.62 H; (**d**) 0.98 H.

2.2.2. Experimental Results for the High-Rise Building in the Urban Environment

Using the wind tunnel experiments, static and fluctuating wind pressure distributions generated by wind blowing onto the front of the high-rise building in the urban environment were analyzed (0°). As mentioned above, the urban area was located in Seoul, Korea. There are various buildings (12–172 m high) arranged around the target building. The results are shown in Figures 14 and 15.

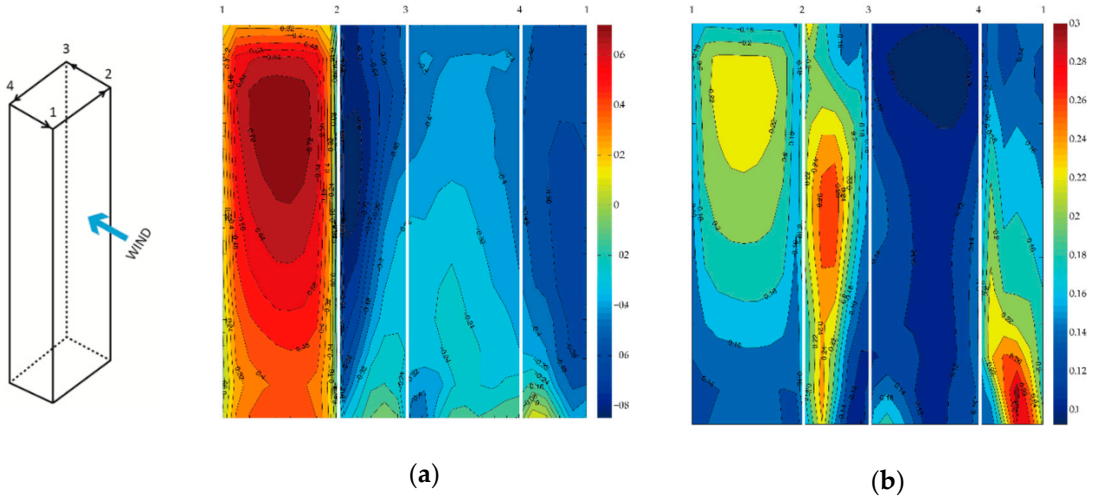

Figure 14. Wind pressure distribution around the high-rise building in the urban environment (0°): (**a**) mean wind pressure coefficient; (**b**) fluctuating wind pressure coefficient.

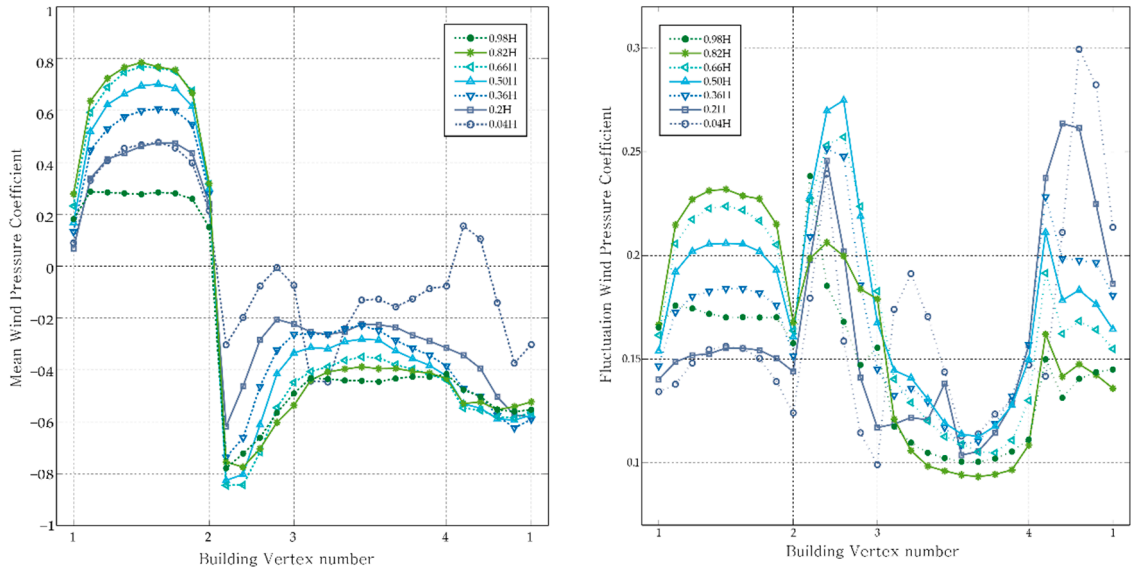

(**a**) (**b**)

Figure 15. Wind pressure coefficient around the high-rise building in the urban environment (0°): (**a**) mean wind pressure coefficient; (**b**) fluctuating wind pressure coefficient.

As per the results of the distribution of mean wind pressure coefficient, the low-height buildings located at the front of the building did not significantly affect the vertical distribution of wind velocity. Therefore, the distribution of the mean wind pressure on side 1–2 was similar to the case of the building without surrounding buildings. Also, the overall aspect of the side was similar to the single building, but a lower negative pressure was observed in the lower parts of sides 2–3, 4–1. It was estimated that the influence of the wind on the lower part was reduced due to the influence of the low-rise building located at the front of the target building.

In the case of fluctuating wind pressure coefficient, irregular results were observed compared to the distribution around the single high-rise building. In the case of side 1–2, the overall aspects were similar, but the results of sides 2–3, 4–1 were different from the case of the building without the surrounding buildings. In case of side 2–3, a high fluctuating wind pressure coefficient was observed in the middle layer. This was estimated to have been caused by the effect of a vortex formed on the upper side of other buildings. This result was unlike that for the distribution of coefficient in the single building. In case of side 4–1, the high fluctuating wind pressure coefficient appeared in the lower part. This result was similar to the distribution of wind pressure distribution in the single building. This result was seen as the result of the placement of low surrounding buildings near side 4–1 of the high-rise building. In the case of side 3–4, an irregular distribution was observed due to the difference between pressure distributions of sides 2–3 and 4–1.

The values (Pa) of the fluctuating wind pressure around the high-rise building were investigated. The values of the pressure were verified at the point where the maximum and minimum RMS values of fluctuating wind pressure coefficient (maximum: point 334, minimum: point 75) were identified. The two points are shown in Figure 16a. Time series data of wind pressure of the two points are shown in Figure 16b. Table 3 gives the pressure values of each point. The overall pressure was primarily negative due to deconfliction occurring at the front and side corners, as for the previous case (without surrounding buildings). The overall value was less than the fluctuating wind pressure generated in the building without surrounding buildings because of the influence of surrounding buildings.

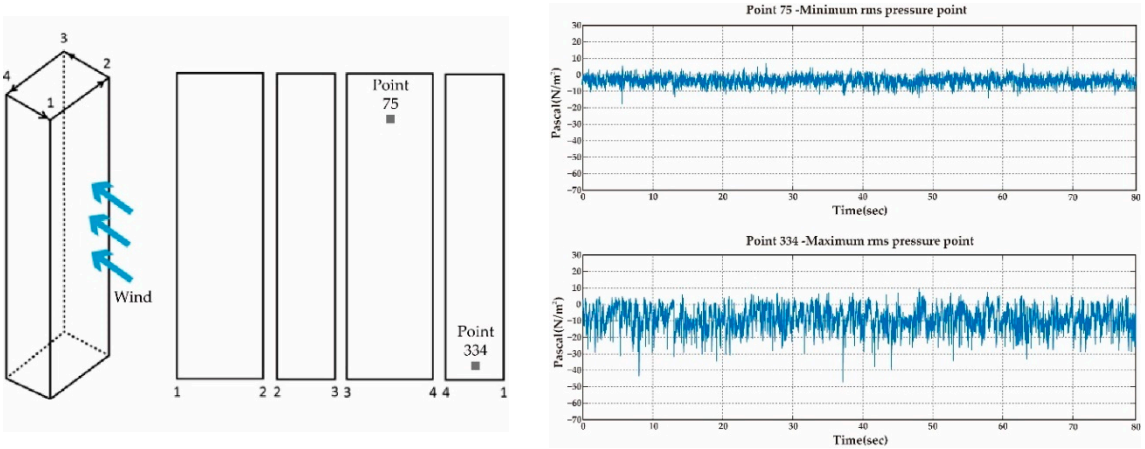

(**a**) (**b**)

Figure 16. The points with the maximum and minimum RMS values of fluctuating wind pressure (the urban environment): (**a**) the locations of the two points; (**b**) pressure data of each point.

Table 3. The pressure values at the points with the maximum and minimum RMS values of fluctuating wind pressure (the urban environment).

Pressure Point	Max Value (Pa)	Min Value (Pa)	RMS Value (Pa)
Point 75 (Minimum)	2.154	−19.75	7.63
Point 334 (Maximum)	11.57	−47.52	10.44

Next, the case of the high-rise building in the urban environment was checked at various angles (30° to 360°). Figures A4–A14 (Appendix B) give the results of pressure distributions of the high-rise building in the urban environment at various angles (30° to 360°). In the case of distribution of the mean wind pressure coefficient, a high value was observed in the upper part of the surface tangential to the wind attack, which was similar to the result obtained for the single building. However, some irregular distributions were observed due to the influence of the surrounding buildings. In the case of fluctuating wind pressure coefficient, unlike the single building which showed a high distribution in the middle and lower parts, most of the high values were shown in the middle part and the upper part of the side tangential to the wind attack. This was a common phenomenon when there was a tall building in front of the target building. As a result, it was found that high fluctuating components were formed in the upper and middle parts due to other high-rise buildings located in front of the target building.

Next, the fluctuating wind pressure around the high-rise building in urban environment was analyzed. The points and the method of analysis were the same as for the analysis of fluctuating wind pressure around the single building. The results of frequency analysis of nine points for each height are shown in Figure 17. In the case of the fluctuating wind pressure around the high-rise building located in the urban environment, the overall power was less than the power of the fluctuating wind pressure around the single building except for a specific point of the high-rise building. In the case of the low parts of the building (0.02 H, 0.36 H), overall, a vibration component at frequencies between 1 and 7.5 Hz dominated. A vibration component having high power was shown for side 4–1. This is because a vortex formed as the wind blowing from the upper part of side 1–2 of the high-rise building flowed to sides 2–3 and 4–1, and the vortex was stagnated by the space formed between the surrounding low-height buildings in the lower layer. Unlike the case of the building without surrounding buildings, the power in the frequency range between 1 Hz and 2.5 Hz was relatively high. In the case of the high parts of the building (0.62 H, 0.98 H), vibration components with frequencies between 1 Hz and 7.5 Hz mainly existed, and relatively high power was observed in the frequency range between 2 and

5 Hz, similar to the lower part. High power was shown for side 2–3 at 0.98 H, attributed to a vortex in the upper part due to the influence of the surrounding high-rise building adjacent to side 2–3. The tendency of the frequency spectrum observed at the upper layer was similar to that at the lower layer. However, overall, the power of the fluctuating wind pressure was shown to be weak.

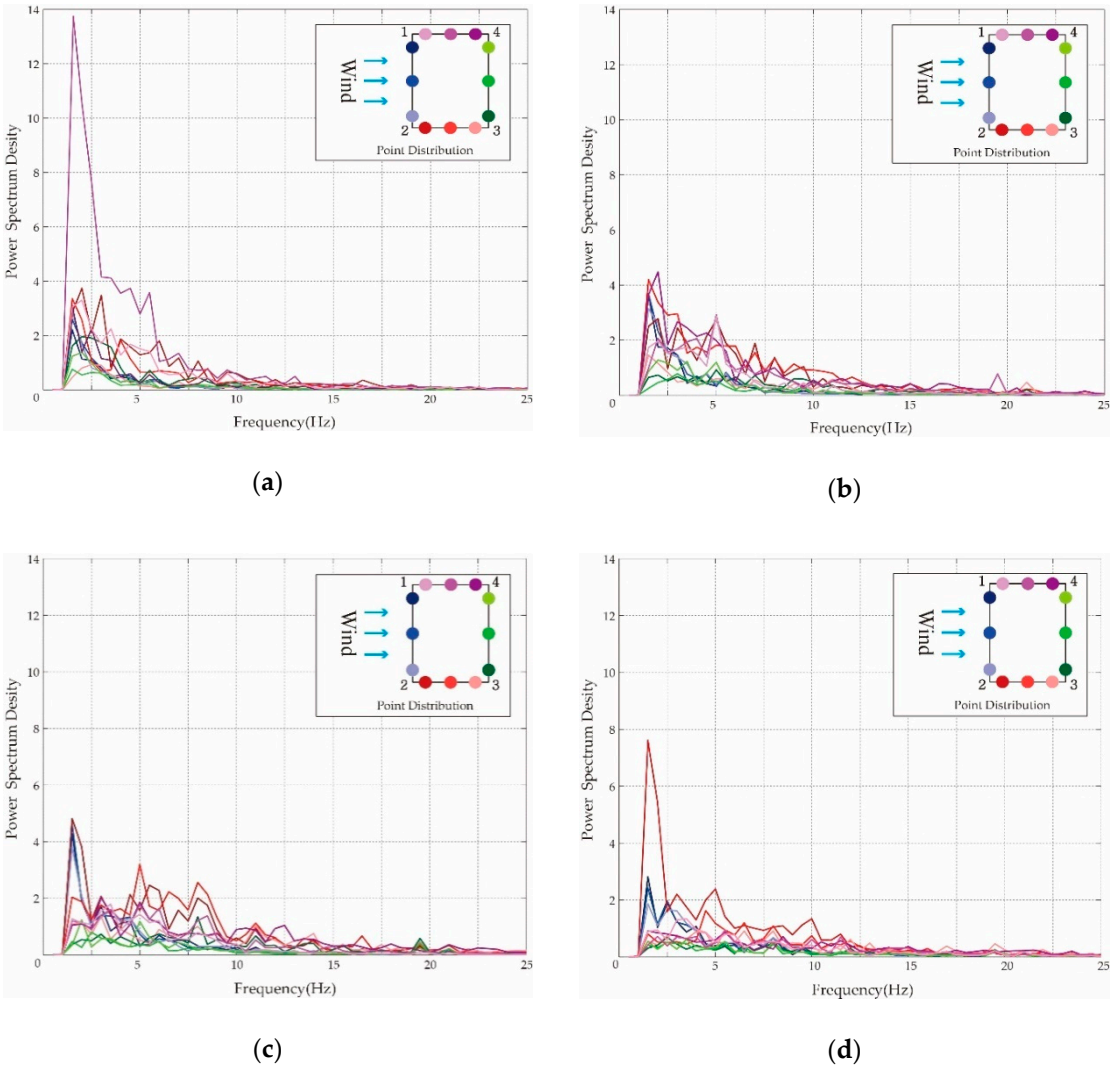

Figure 17. Frequency spectrum of fluctuating wind pressure (the urban environment): (**a**) 0.02 H; (**b**) 0.36 H; (**c**) 0.62 H; (**d**) 0.98 H.

As shown in the above results, fluctuating wind pressure with vibration components between 1 and 7.5 Hz was generally distributed around the high-rise building. Also, when there was a high-rise building with a height similar to that of the target building in the vicinity, fluctuating wind pressure with high power was formed on the upper part. Basically, fluctuating wind pressure is influenced by various factors such as the atmospheric viscosity, the surrounding environment, and the shape of building [36]. The frequency range of fluctuating wind pressure around the rectangular high-rise buildings surrounded by the atmosphere was expected to be basically similar to the experimental results. In addition, frequency analysis of the fluctuating wind pressure formed by the wind blowing at angles of attack from 30 ° to 330 ° onto the high-rise building was carried out. However, there were no significant differences found for the frequency range of the fluctuating wind pressure. Because of this reason, the results were omitted.

3. Feasibility Study of Fluctuating Wind Pressure around the High-Rise Building

Generally, wind energy is assessed using the wind power density. The wind power density is the value that can be obtained from the measured mean wind speed [37]. However, since fluctuating wind pressure is formed by the wind speed changing with time, it cannot be assessed using the general wind power density calculated for a mean wind speed. The fluctuating wind pressure induces vibration energy, which can be converted to electrical energy through energy-harvesting devices. Recently, the theory of energy-harvesting devices using vibration energy as established, and various types of devices were designed [38].

In this section, an analytical model for a simple vibration-based energy-harvesting device using fluctuating wind pressure was set up, and the feasibility of fluctuating wind pressure formed around the high-rise building as an energy-harvesting source was evaluated using the analytical model. The energy-harvesting device for the analytical model was an electromagnetic-based spring mass damper system. The fluctuating wind pressure that varied with time formed vibration which directly excited the system. Considering that the energy-harvesting device was installed on the side of the high-rise building, the electromagnetic method was selected because this device has a potentially high conversion efficiency and a simple resonator structure, which can be used for low frequencies [39]. Additionally, because the purpose of this study was to understand the feasibility of fluctuating wind pressure around the high-rise building as an energy source rather than developing a sophisticated energy-harvesting device, the analytical model for the single-degree-of-freedom (SDOF) system, which can be easily applied to a wide range of high-rise buildings, was utilized.

For the analytical model, the equation of motion for a generalized SDOF system with excitation of fluctuating wind pressure was utilized. The fluctuating wind pressure used for the analysis was obtained from the pressure data measured from 364 wind pressure taps through the previous wind tunnel test. Next, the voltage was calculated using the velocity obtained from the equation of motion and electromagnetic induction formulas that reflect the specifications of the coil and magnet. Based on the calculated voltage, an electrical circuit was designed, from which the power was calculated. The electric circuit of the proposed device was designed to reflect a Thevenin-equivalent circuit and to obtain the maximum power by setting the same value of the coil resistance and the load resistance of the battery. The efficiency of the energy-harvesting device utilized in the analytical model was set to 50%, considering previous studies [40]. Figure 18a shows the concept of energy-harvesting for the analytical model to be used in this study.

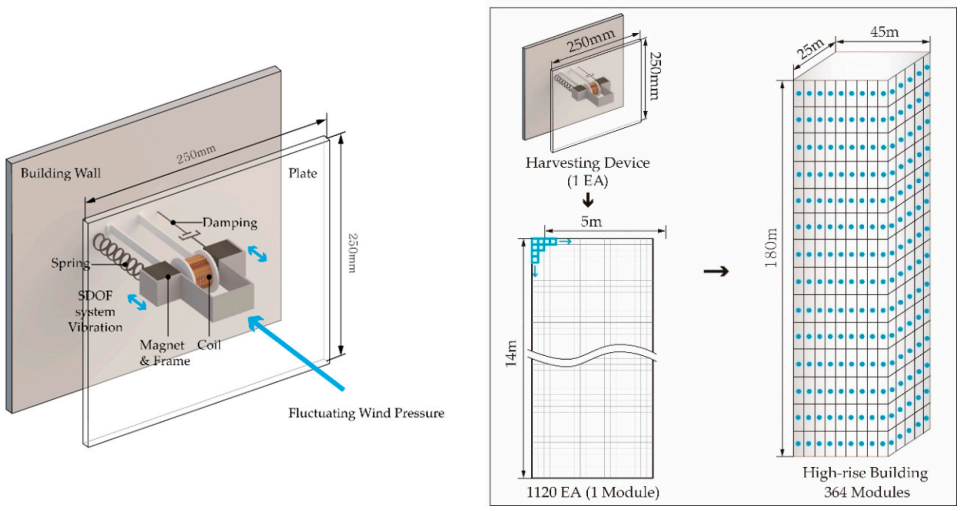

(**a**) (**b**)

Figure 18. (**a**) Conceptual diagram of the energy-harvesting system for the analytical model; (**b**) conceptual diagram of the placement of modules to calculate electricity in the entire building area.

The specifications of the magnets and coils used in the electromagnetic energy-harvesting device for the analytical model were considered. In the case of magnets, neodymium magnets were used, and magnetic flux was considered according to the size of the magnets. For the coil, the diameter of the coil, the number of turns, and the resistance of the coil were set. Also, the mass and spring characteristics of the system were set. The system was designed to have a resonance frequency (6.7 Hz) suitable for the frequency range of the fluctuating wind pressure. In the case of mass, the mass value was calculated considering the plate receiving the external force of the fluctuating wind pressure, the weight of the magnet, and the frame connecting the plate and the magnet. The stiffness of the spring was set in consideration of the resonance frequency. The damping ratio values formed by the mass and spring of the set system were calculated. The specifications of the vibrating energy-harvester are shown in Tables 4 and 5.

Table 4. Specifications of the energy-harvesting system I.

Plate Size (mm^3)	Plate Weight (g)	Magnet Frame Weight (g)	Spring Stiffness	Damping Ratio
250 × 250 × 6	825	710	2900	0.02

Table 5. Specifications of system II.

Magnet Size (mm^3)	Magnet Weight (g)	Magnet Flux (T)	Diameter of the Coil Wire (mm)	Turns of Coil	Resistance of Coil (Ω)
30 × 30 × 30	65	0.265	0.45	1380	10.56

The output voltage and power at the angle of wind attack of 0° were calculated from the analytical model. The converted voltage is shown in Figures 19 and 20. The results showed that the points with maximum and minimum RMS values of fluctuating wind pressure were different from the points with maximum and minimum RMS values of voltage. This was due to the resonance frequency of the energy-harvesting device utilized in the analytical model. In addition, the power from the energy-harvesting device with 50% efficiency was calculated. As the result of calculation, a maximum power of 0.1469 W and a minimum power of 0.0013 W were produced around the building without surrounding buildings. In the urban environment, a maximum power of 0.0778 W and a minimum power of 0.0007 W were generated. The quantitative results of calculated voltage and power are shown in Tables 6 and 7.

Additionally, applying the above procedure, the total converted power at the angle of wind attack of 0° was calculated when the proposed energy-harvesting device was utilized throughout the entire building area. In order to effectively simulate the power, the area corresponding to each wind pressure tap was defined as one module (14 × 5 m^2), reflecting the size of the building (45 × 25 × 180 m^3). Then, the total power of 364 modules was calculated considering the energy-harvesting area of each module. The device could not be installed in the whole area; however, this analysis made sense in terms of checking the maximum available power. The placement of the modules to calculate electricity in the entire building area is shown in Figure 18b. The power per module, calculated from the analytical model of the energy-harvesting device, which uses the excitation force of the fluctuating wind pressure formed by the wind at an angle of attack of 0°, is shown in Figures 21 and 22. Also, the calculated power converted by the energy-harvesting device throughout the entire high-rise building area is shown in Table 8.

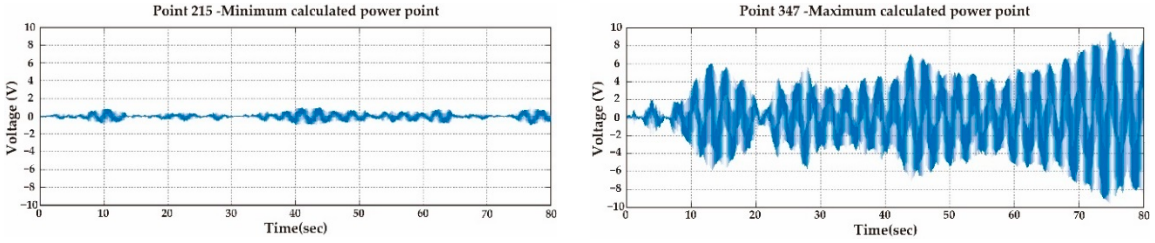

(**a**) (**b**)

Figure 19. Calculated voltage converted by the energy-harvesting device around the high-rise building without surrounding buildings (angle of wind attack: 0°): (**a**) minimum calculated power point (point 215); (**b**) maximum calculated power point (point 347).

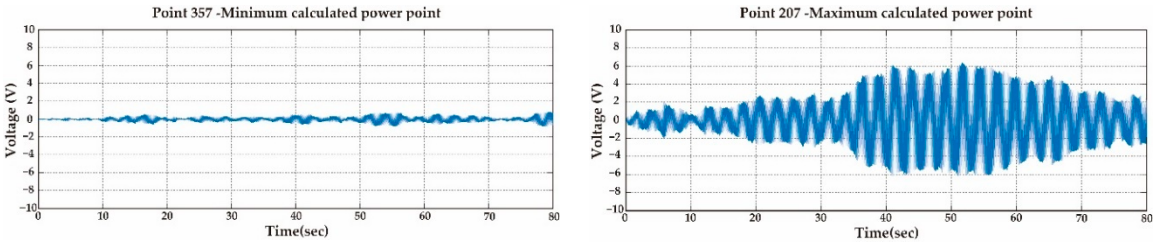

(**a**) (**b**)

Figure 20. Calculated voltage converted by the energy-harvesting device around the high-rise building in the urban environment (angle of wind attack: 0°): (**a**) minimum calculated power point (point 357); (**b**) maximum calculated power point (point 207).

Table 6. Calculated voltage and power converted by the energy-harvesting device around the high-rise building without surrounding buildings (angle of wind attack: 0°).

Case	Maximum Voltage (V)	RMS Voltage (V)	Power Considering 50% Efficiency of the Device (W)
Minimum calculated power point (point 215)	1.0156	0.3397	0.0013
Maximum calculated power point (point 347)	9.5867	3.5233	0.1469

Table 7. Calculated voltage and power converted by the energy-harvesting device around the high-rise building in the urban environment (angle of wind attack: 0°).

Case	Maximum Voltage (V)	RMS Voltage (V)	Power Considering 50% Efficiency of the Device (W)
Minimum calculated power point (point 357)	0.7898	0.2473	0.0007
Maximum calculated power point (point 207)	6.1765	2.5636	0.0778

Table 8. Calculated power converted by the energy-harvesting device throughout the entire high-rise building area (angle of wind attack: 0°).

Case	Produced Power in the Entire Area (W)	Maximum Power Per Single Module (W)	Minimum Power Per Single Module (W)
Case I: without surrounding buildings	13,002.39	164.58	1.525
Case II: in the urban environment	4963.26	87.13	0.81

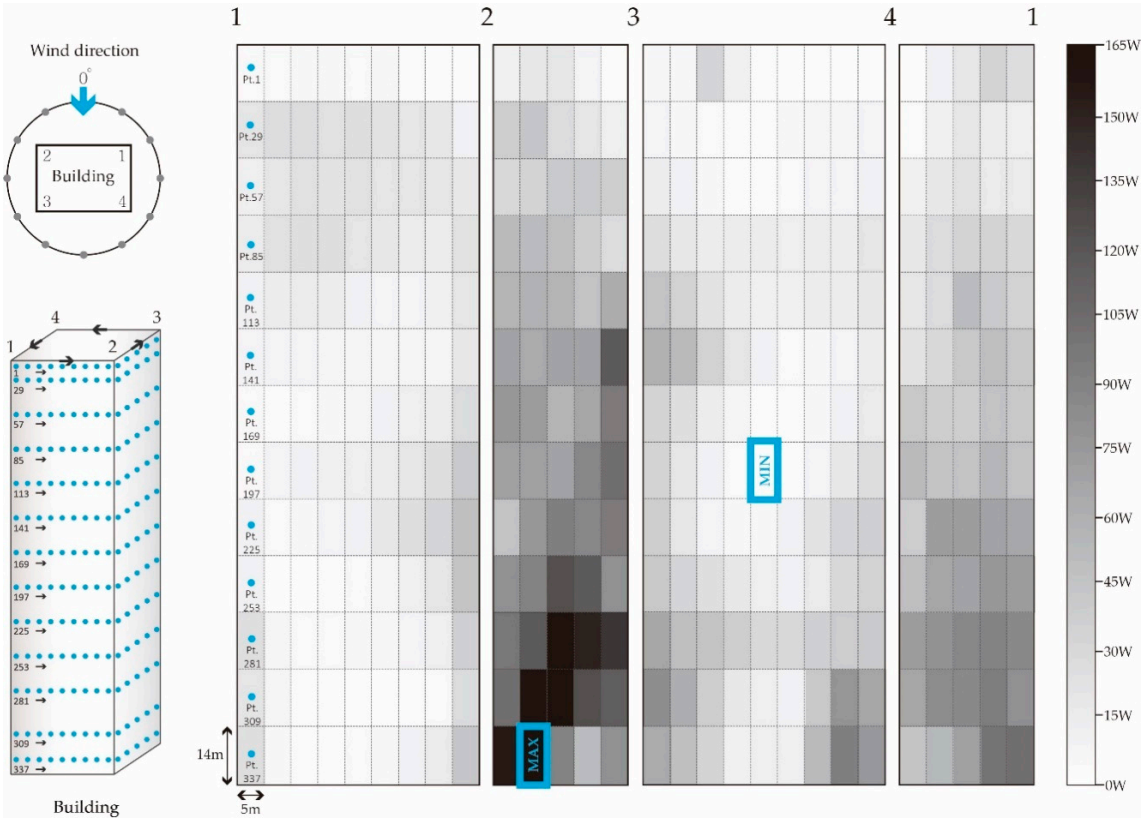

Figure 21. Distribution of the calculated power caused by the fluctuating wind pressure generated around the high-rise building without surrounding buildings (angle of wind attack: 0°).

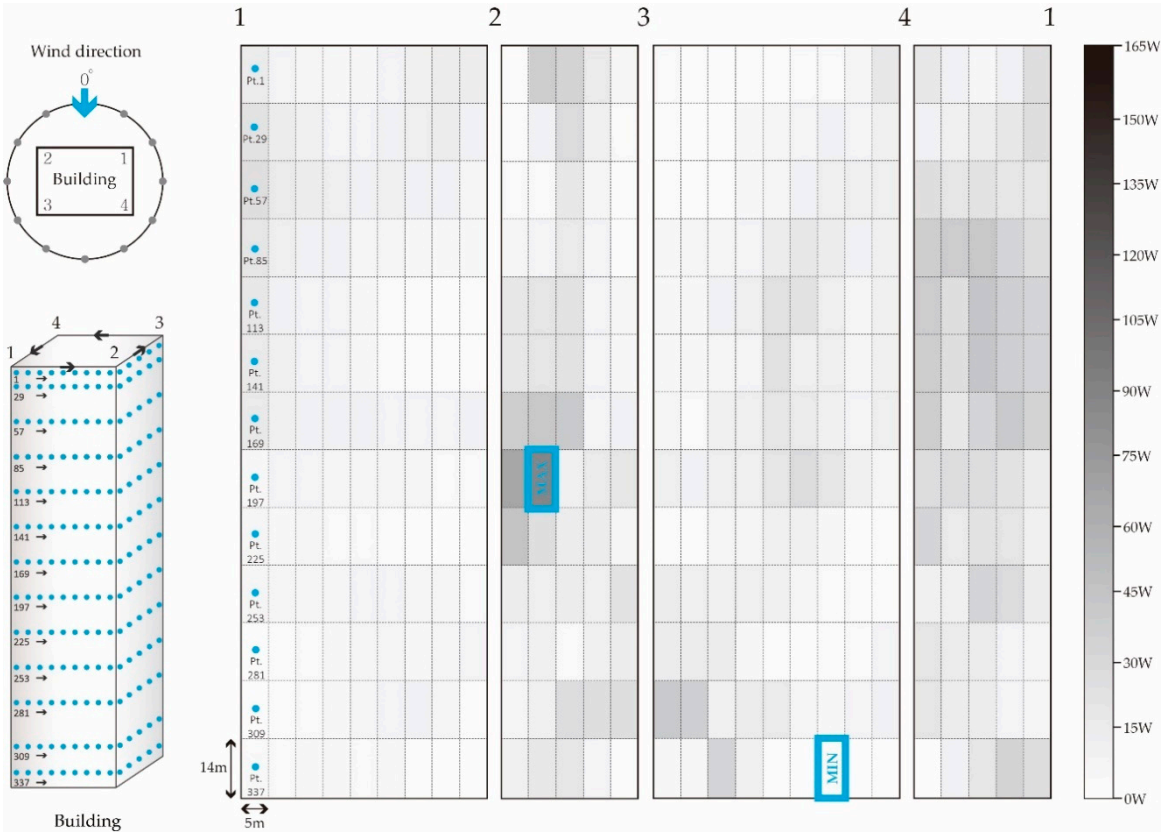

Figure 22. Distribution of the calculated power caused by the fluctuating wind pressure generated around the high-rise building in the urban environment (angle of wind attack: 0°).

In the case of the high-rise building without surrounding buildings, the distribution of the calculated power was similar to the distribution of the fluctuating wind pressure. The maximum power was generated at the low part of side 2–3. The minimum power was generated at the middle part of side 3–4. For buildings located in urban areas, the maximum power was found in the middle part of side 2–3, and the minimum power was found in the high part of side 1–2. Unlike the distribution of the fluctuating wind pressure, relatively low power was obtained for the lower part of side 4–1. This is the phenomenon that occurs when the resonance frequency of the device does not coincide with the frequency of the fluctuating wind pressure formed in the lower part of side 4–1.

Additionally, the result of output power for wind blowing from various angles using the same analysis model is shown in Figure 23. As a result, higher power was generated around the single building without the influence of surrounding buildings, and the highest energy was generated by wind blowing at the angle of attack of 0°. In addition, to compare the power values obtained from the top and bottom of the high-rise buildings, the power values obtained in the upper and lower areas based on the height of 0.5 H were calculated and compared. As a result of the comparison, in the case of the high-rise building without surrounding buildings, higher energy was obtained from the lower part at a rate of 60.71% of the total when averaging all cases. For buildings located in the urban environment, lower energy could be obtained from the bottom part at a rate of 42.17% of the total. This shows that, when there are additional high-rise buildings around the target high-rise building, the power that can be obtained around the high-rise building becomes smaller. In particular, the amount of power that can be obtained at the lower part of the building becomes smaller. This is due to the fact that the overall wind intensity is weakened, and the generated vortex does not go down to the bottom due to the influence of surrounding buildings.

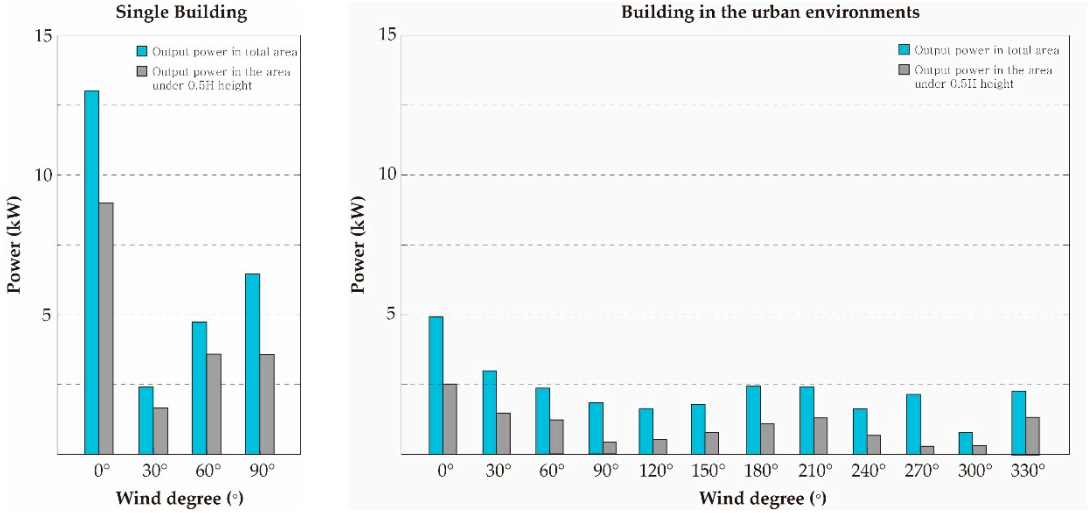

(**a**) (**b**)

Figure 23. The calculated power using fluctuating wind pressure generated around the high-rise building (based on the angle of wind attack): (**a**) without surrounding buildings; (**b**) in the urban environment.

The value of power obtained from the fluctuating wind pressure formed around the high-rise building, obtained through the simulation, was less efficient than the power generated by the wind turbines used on the market. However, electricity can be obtained by fluctuating wind pressure in places where wind turbines cannot be used. In addition, it is considered that fluctuating wind pressure is valuable as an energy-harvesting source because it can obtain sufficient energy compared to the electric energy obtained from existing energy-harvesting systems. However, the device applied to the analytical model was not optimized for maximum efficiency. Therefore, in order to achieve maximum efficiency, the characteristics of fluctuating wind pressure should be effectively reflected, and the optimized specifications of the device should be considered. Furthermore, the performance of the device should be verified through implementation and experimentation of the considered device, and further study for practical use is required.

4. Conclusions

In this study, the wind pressure distribution around high-rise buildings was studied using the wind tunnel test to analyze the feasibility of fluctuating wind pressure as a new energy-harvesting source. For the analysis, the distributions of static and fluctuating wind pressure were considered to comprehensively understand the characteristics of the fluctuating wind pressure as an energy source. The results of the wind pressure distribution obtained from the experiment are as follows:

- High-rise building without surrounding buildings

In the case of static pressure, the results showed the highest positive pressure on the upper part (0.8 H) of the front surface that comes in contact with the blowing wind. The highest negative pressure was observed on the lower part of the side surface. In the case of fluctuating wind pressure, the highest fluctuating component was observed on the middle and low parts.

- High-rise building in the urban environment

In the case of static pressure, high pressure was formed on the high part of the surface in contact with the angle of wind attack. In the case of fluctuating wind pressure, high energy was generally formed on the high and middle parts of the building when affected by other high-rise buildings with

a height similar to the target building. On the other hand, when affected by low buildings, high fluctuating wind pressure was observed in the low part of the building.

Generally, the fluctuating wind pressure around a single high-rise building varies depending on the shape of the building. However, in the case of a typical single high-rise building shaped like a rectangular parallelepiped, the experimental results can be used as reference data to utilize fluctuating wind pressure around the high-rise building as a new energy-harvesting source. In the case of fluctuating wind pressure around the high-rise building in urban environments, the distribution is not constant, because environments around high-rise buildings are different. For this reason, it is difficult to use the results of this study as an absolute reference. However, the results of this study show that fluctuating wind pressure can vary from the low part to the high part of a building. The experimental results show that there is a possibility to acquire electric energy through fluctuating wind pressure in new areas of high-rise buildings, different from places where the existing small wind turbines are installed (rooftops and corners of high-rise buildings).

In addition, in order to evaluate fluctuating wind pressure as a valuable new energy-harvesting source, an analytical model of a simple energy-harvesting device was utilized. As a result of evaluation using the analysis model, it is considered that fluctuating wind pressure could be sufficiently utilized as an energy-harvesting source because it obtains sufficient power compared with conventional energy-harvesting systems. The results of this study can be used for the development of new types of energy-harvesting devices that can be installed in locations different from conventional wind turbine systems used around high-rise buildings. However, further study is necessary to optimize the device considering the characteristics of fluctuating wind pressure to effectively utilize fluctuating wind pressure around high-rise buildings. Currently, a study is underway to develop new types of energy-harvesting devices that reflect these challenges.

Author Contributions: J.-C.P. was the principal researcher of this work. He conducted the numerical and experimental research. I.-H.K. assisted with the experiments and data analysis. H.-J.J. supervised the research.

Acknowledgments: This work was supported by a National Research Foundation of Korea (NRF) grant funded by the Korean government (MSIP) (No. 2017R1A5A1014883).

Conflicts of Interest: The authors declare no conflicts of interest.

Appendix A Pressure Distribution on the High-Rise Building without Surrounding Buildings

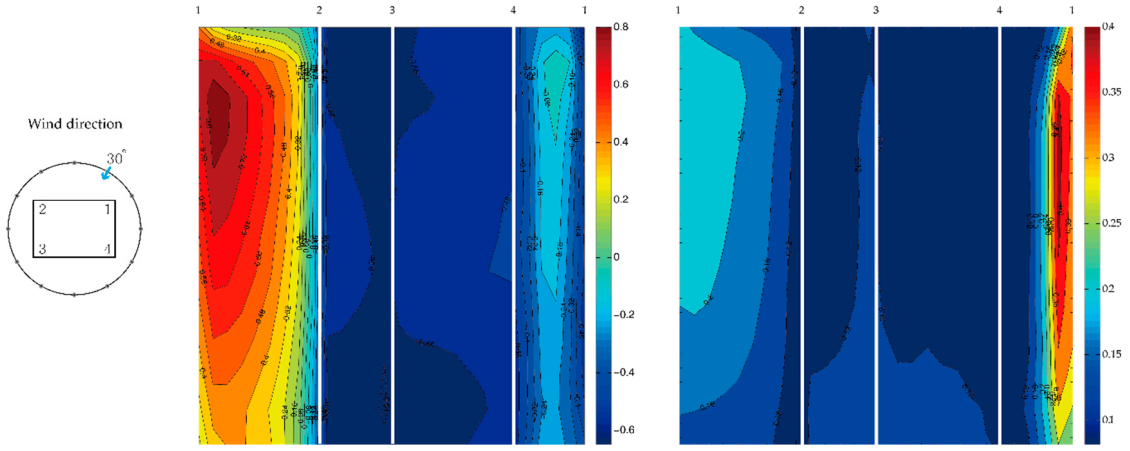

(**a**) (**b**) (**c**)

Figure A1. Pressure coefficient distribution (30°): (**a**) angle of wind attack; (**b**) mean pressure coefficient; (**c**) fluctuating pressure coefficient.

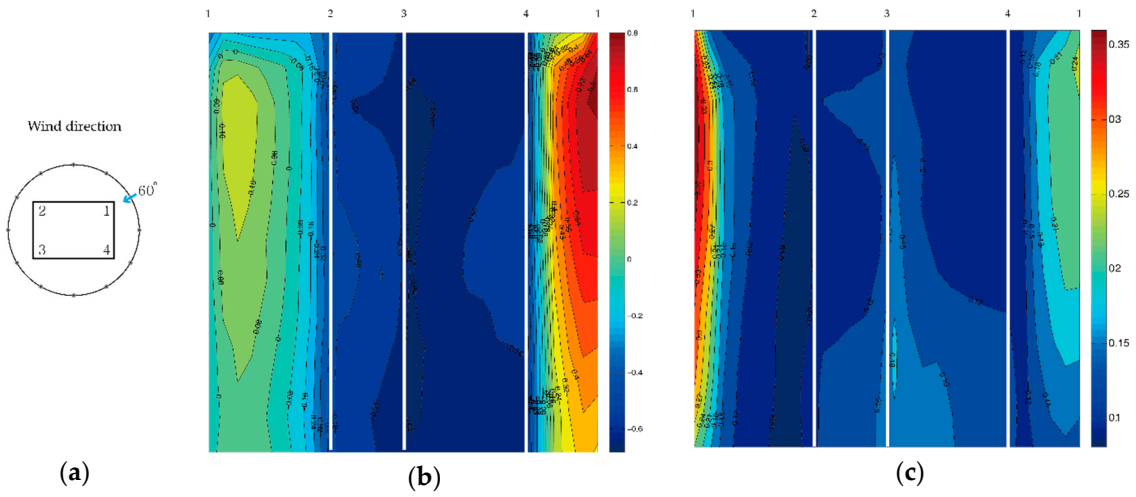

(**a**) (**b**) (**c**)

Figure A2. Pressure coefficient distribution (60°): (**a**) angle of wind attack; (**b**) mean pressure coefficient; (**c**) fluctuating pressure coefficient.

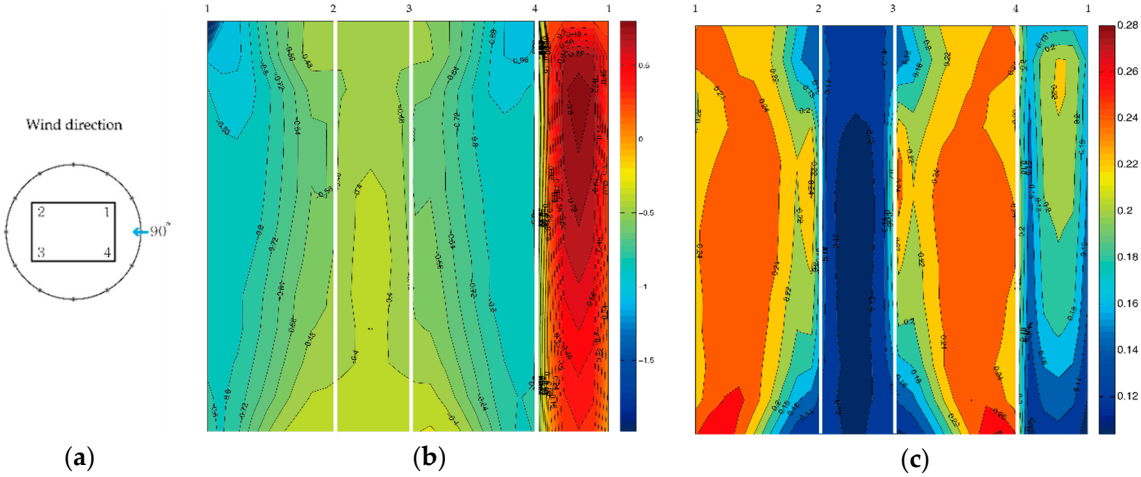

(**a**) (**b**) (**c**)

Figure A3. Pressure coefficient distribution (90°): (**a**) angle of wind attack; (**b**) mean pressure coefficient; (**c**) fluctuating pressure coefficient.

Appendix B Pressure Distribution of the High-Rise Building in the Urban Environment

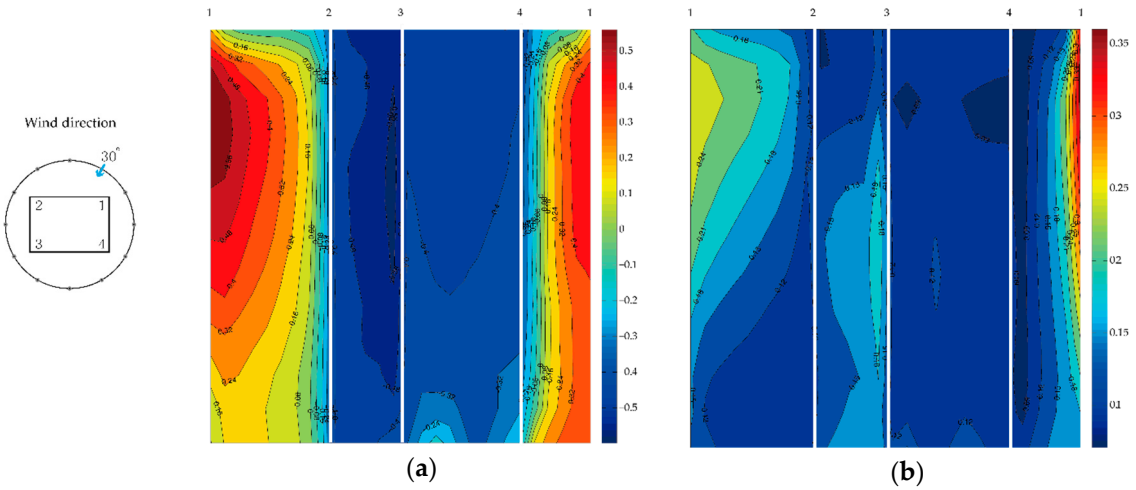

Figure A4. Pressure coefficient distribution (30°): (**a**) angle of wind attack; (**b**) mean pressure coefficient; (**c**) fluctuating pressure coefficient.

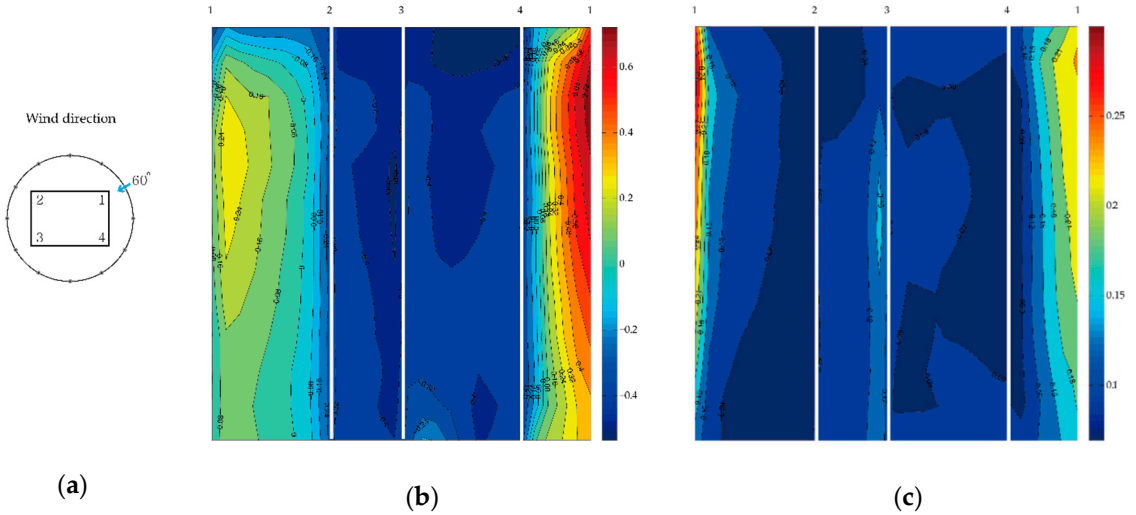

Figure A5. Pressure coefficient distribution (60°): (**a**) angle of wind attack; (**b**) mean pressure coefficient; (**c**) fluctuating pressure coefficient.

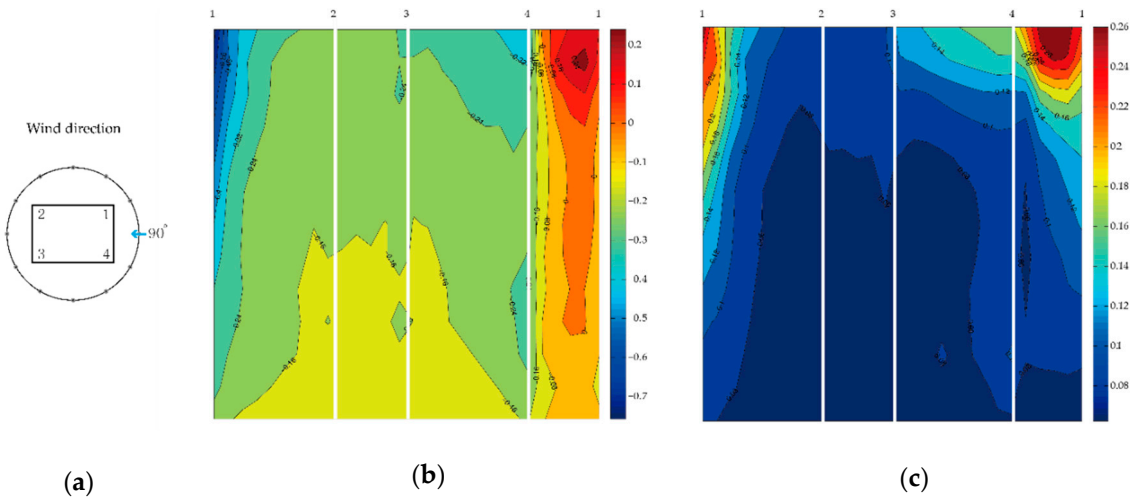

Figure A6. Pressure coefficient distribution (90°): (**a**) angle of wind attack; (**b**) mean pressure coefficient; (**c**) fluctuating pressure coefficient.

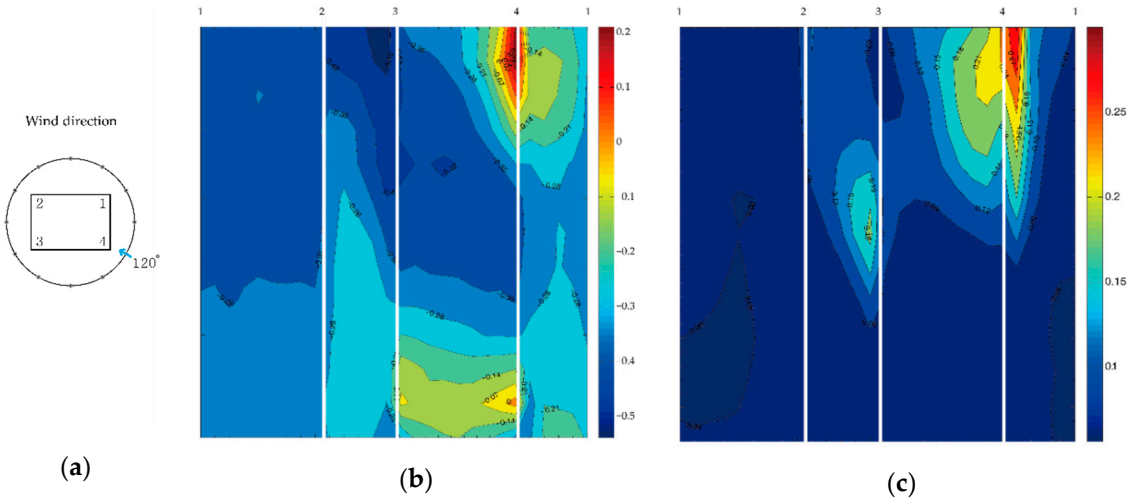

Figure A7. Pressure coefficient distribution (120°): (**a**) angle of wind attack; (**b**) mean pressure coefficient; (**c**) fluctuating pressure coefficient.

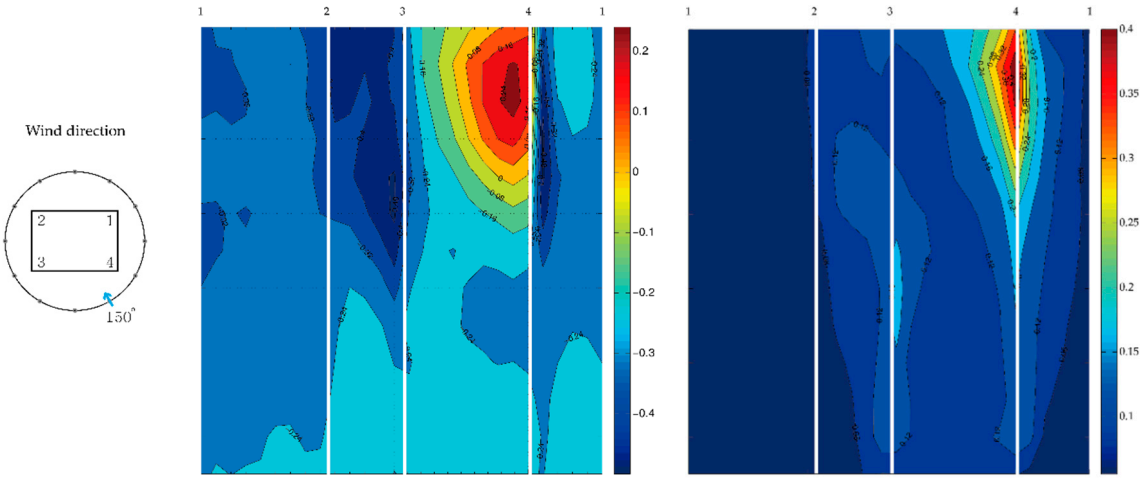

(**a**) (**b**) (**c**)

Figure A8. Pressure coefficient information (150°): (**a**) angle of wind attack; (**b**) mean pressure coefficient; (**c**) fluctuating pressure coefficient.

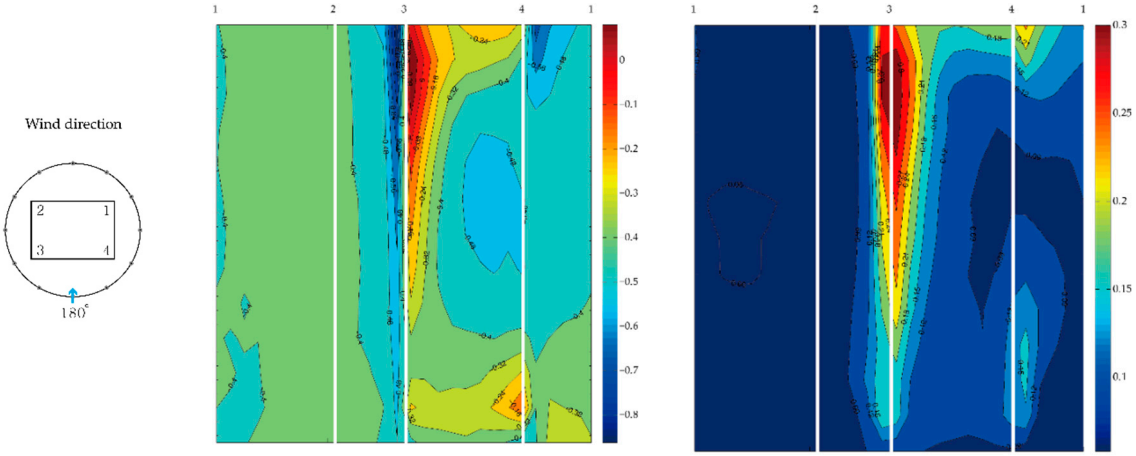

(**a**) (**b**) (**c**)

Figure A9. Pressure coefficient distribution (180°): (**a**) angle of wind attack; (**b**) mean pressure coefficient; (**c**) fluctuating pressure coefficient.

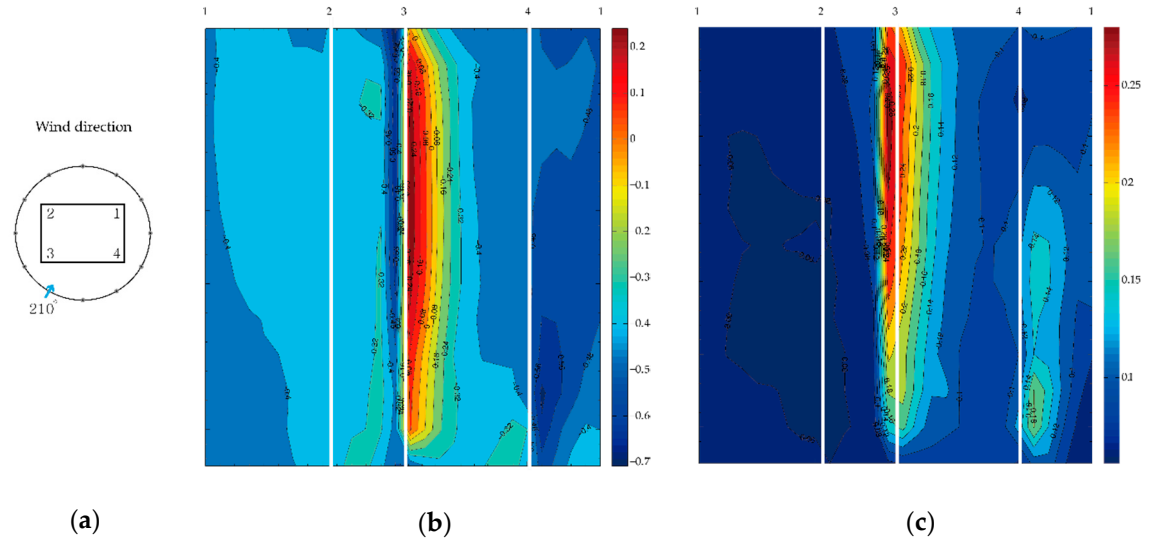

Figure A10. Pressure coefficient distribution (210°): (**a**) angle of wind attack; (**b**) mean pressure coefficient; (**c**) fluctuating pressure coefficient.

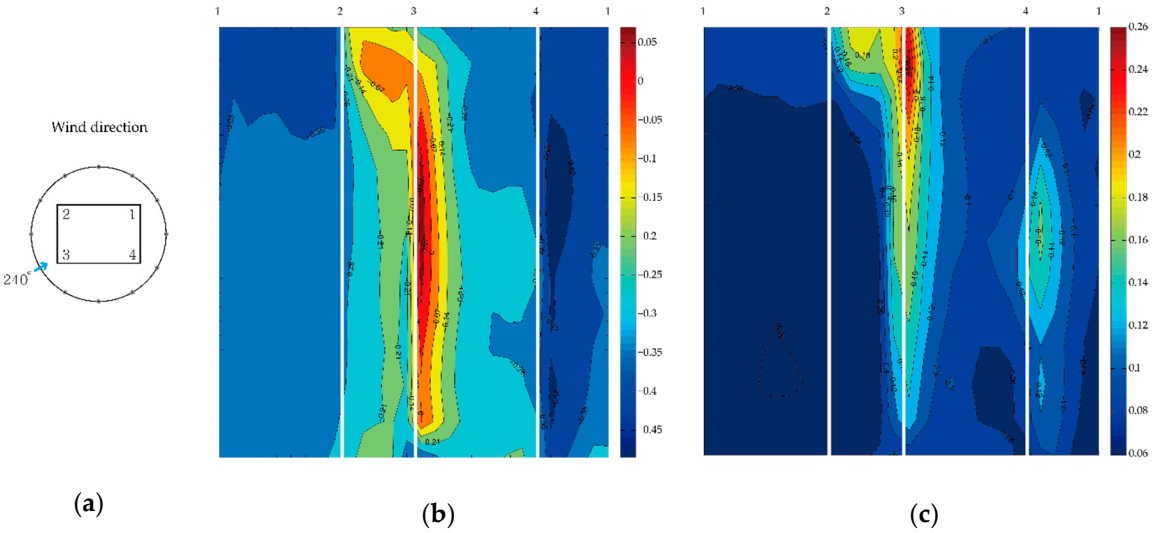

Figure A11. Pressure coefficient distribution (240°): (**a**) angle of wind attack; (**b**) mean pressure coefficient; (**c**) fluctuating pressure coefficient.

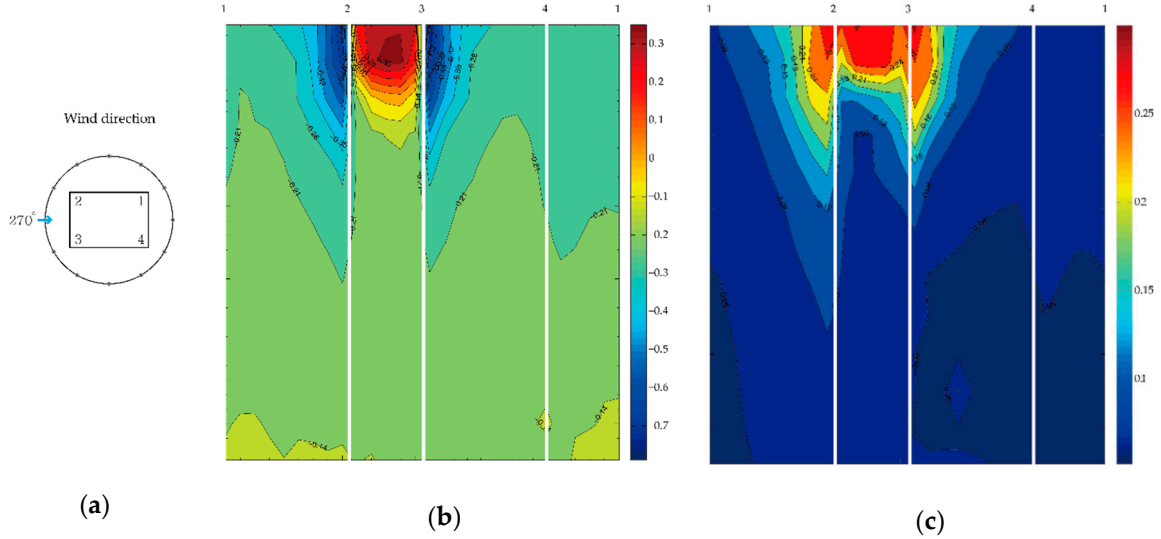

(**a**) (**b**) (**c**)

Figure A12. Pressure coefficient distribution (270°): (**a**) angle of wind attack; (**b**) mean pressure coefficient; (**c**) fluctuating pressure coefficient.

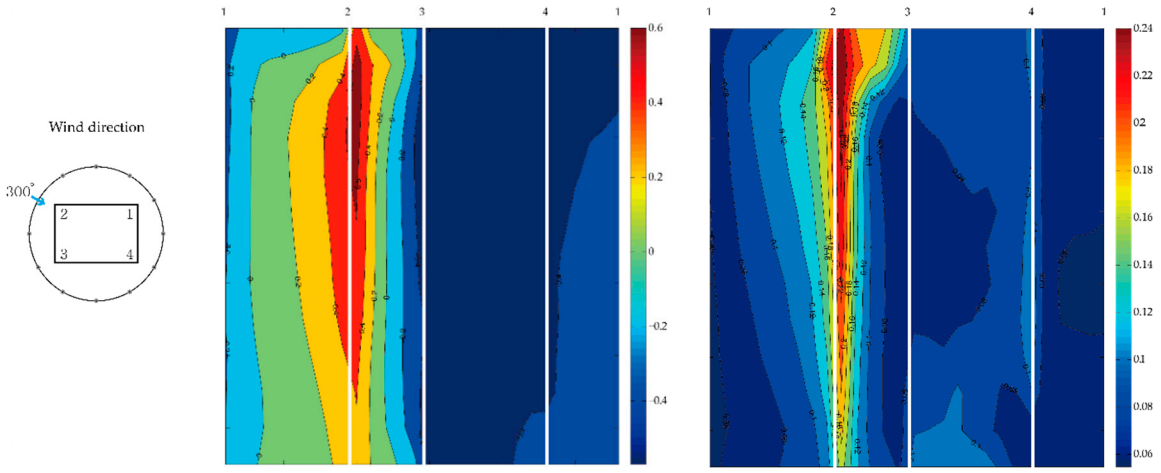

(**a**) (**b**) (**c**)

Figure A13. Pressure coefficient distribution (300°): (**a**) angle of wind attack; (**b**) mean pressure coefficient; (**c**) fluctuating pressure coefficient.

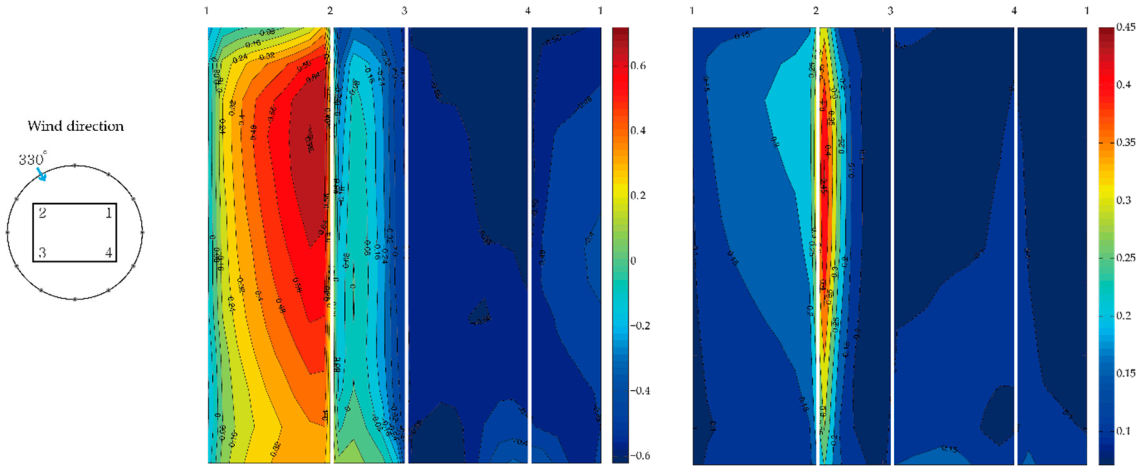

(**a**) (**b**) (**c**)

Figure A14. Pressure coefficient distribution (330°): (**a**) angle of wind attack; (**b**) mean pressure coefficient; (**c**) fluctuating pressure coefficient.

References

1. Jain, P. *Wind Energy Engineering*; McGraw-Hill: New York, NY, USA, 2011; p. 330.
2. De Alencar, D.B.; Affonso, C.D.; de Oliveir, R.C.L.; Rodriguez, J.L.M.; Leite, J.C.; Reston, J.C. Different Models for Forecasting Wind Power Generation: Case Study. *Energies* **2017**, *10*, 1976. [CrossRef]
3. Manwell, J.F.; McGowan, J.G.; Rogers, A.L. *Wind Energy Explained: Theory, Design and Application*; John Wiley & Sons: Hoboken, NJ, USA, 2010.
4. Campbell, N. *Wind Energy for the Built Environment (Project WEB): Assessment of Wind Energy Utilisation Potential in Moderately Windy Built-up Areas*; BDSP: London, UK, 2001.
5. Smith, R.F.; Killa, S. Bahrain world trade center (BWTC): The first large-scale integration of wind turbines in a building. *Struct. Des. Tall Spec. Bulid.* **2007**, *16*, 429–439. [CrossRef]
6. Al-Kodmany, M.K. Green towers and iconic design: Cases from three continents. *Int. J. Archit. Res. ArchNet-IJAR* **2014**, *8*, 11–28. [CrossRef]
7. Cowan, D. Strata SE1, London—Propelling sustainable regeneration. *Proc. Inst. Civ. Eng.* **2010**, *163*, 56–63. [CrossRef]
8. Pitteloud, J.; Gsänger, S. *Small Wind World Report Summary*; World Wind Energy Association (WWEA): Bonn, Germany, 2017.
9. McTavish, S.; Feszty, D.; Sankar, T. Steady and rotating computational fluid dynamics simulations of a novel vertical axis wind turbine for small-scale power generation. *Renew. Energy* **2012**, *41*, 171–179. [CrossRef]
10. Abdalrahman, G.; Melek, W.; Lien, F.S. Pitch angle control for a small-scale Darrieus vertical axis wind turbine with straight blades (H-Type VAWT). *Renew. Energy* **2017**, *114*, 1353–1362. [CrossRef]
11. Jin, X.; Wang, Y.M.; Ju, W.B.; He, J.; Xie, S.Y. Investigation into parameter influence of upstream deflector on vertical axis wind turbines output power via three-dimensional CFD simulation. *Renew. Energy* **2018**, *115*, 41–53. [CrossRef]
12. Sharpe, T.; Proven, G. Crossflex: Concept and early development of a true building integrated wind turbine. *Energy Build.* **2010**, *42*, 2365–2375. [CrossRef]
13. Chong, W.T.; Poh, S.C.; Fazlizan, A.; Pan, K.C. Vertical axis wind turbine with omni-directional-guide-vane for urban high-rise buildings. *J. Cent. South Univ.* **2012**, *19*, 727–732. [CrossRef]
14. Tjiu, W.; Marnoto, T.; Mat, S.; Ruslan, M.H.; Sopian, K. Darrieus vertical axis wind turbine for power generation I: Assessment of Darrieus VAWT configurations. *Renew. Energy* **2015**, *75*, 50–67. [CrossRef]
15. Bayoumi, M.; Fink, D.; Hausladen, G. Extending the feasibility of high-rise façade augmented wind turbines. *Energy Build.* **2013**, *60*, 12–19. [CrossRef]
16. Park, J.; Jung, H.-J.; Lee, S.-W.; Park, J. A new building-integrated wind turbine system utilizing the building. *Energies* **2015**, *8*, 11846–11870. [CrossRef]

17. Hassanli, S.; Kwok, K.C.; Zhao, M. Performance assessment of a special Double Skin Façade system for wind energy harvesting and a case study. *J. Wind Eng. Ind. Aerodyn.* **2018**, *175*, 292–304. [CrossRef]
18. Meng, F.Q.; He, B.J.; Zhu, J.; Zhao, D.X.; Darko, A.; Zhao, Z.Q. Sensitivity analysis of wind pressure coefficients on CAARC standard tall buildings in CFD simulations. *J. Build. Eng.* **2018**, *16*, 146–158. [CrossRef]
19. Zhao, D.X.; He, B.J. Effects of architectural shapes on surface wind pressure distribution: Case studies of oval-shaped tall buildings. *J. Build. Eng.* **2017**, *12*, 219–228. [CrossRef]
20. Kim, Y. Pressure fluctuations on a tall building with square cross-section. In Proceedings of the International Symposium 1st Wind and Structures for the 21st Century, Cheju, Korea, 26–28 January 2000; pp. 393–406.
21. Scanivalve Corporation. *ZOC 33/64Px—Electronic Pressure Scanning Module, Instruction and Service Manual*; Scanivalve Corporation: Liberty Lake, WA, USA, 2003.
22. Cao, B.C.; Sarkar, P.P. Time-Domain Aeroelastic Loads and Response of Flexible Bridges in Gusty Wind: Prediction and Experimental Validation. *J. Eng. Mech.* **2013**, *139*, 359–366. [CrossRef]
23. Jakobsen, J.B.; Andersen, T.L.; Macdonald, J.H.G.; Nikitas, N.; Larose, G.L.; Savage, M.G.; McAuliffe, B.R. Wind-induced response and excitation characteristics of an inclined cable model in the critical Reynolds number range. *J. Wind Eng. Ind. Aerodyn.* **2012**, *110*, 100–112. [CrossRef]
24. Mishra, A.R.; James, D.L.; Letchford, C.W. Physical simulation of a single-celled tornado-like vortex, Part B: Wind loading on a cubical model. *J. Wind Eng. Ind. Aerodyn.* **2008**, *96*, 1258–1273. [CrossRef]
25. Pindado, S.; Meseguer, J.; Franchini, S. Influence of an upstream building on the wind-induced mean suction on the flat roof of a low-rise building. *J. Wind Eng. Ind. Aerodyn.* **2011**, *99*, 889–893. [CrossRef]
26. Stull, R.B. *An Introduction to Boundary Layer Meteorology*; Springer Science & Business Media: Berlin, Germany, 2012; Volume 13.
27. Touma, J.S. Dependence of the wind profile power law on stability for various locations. *J. Air Pollut. Control Assoc.* **1977**, *27*, 863–866. [CrossRef]
28. Counihan, J. Adiabatic atmospheric boundary layers: A review and analysis of data from the period 1880–1972. *Atmos. Environ.* **1975**, *9*, 871–905. [CrossRef]
29. Hsu, S.; Meindl, E.A.; Gilhousen, D.B. Determining the power-law wind-profile exponent under near-neutral stability conditions at sea. *J. Appl. Meteorol.* **1994**, *33*, 757–765. [CrossRef]
30. Ougiya, N.; Kanda, M. Simulation of wind force acting on super-high-rise building in passing typhoon. *Procedia Eng.* **2017**, *199*, 3139–3144. [CrossRef]
31. Sun, X.; Liu, H.; Su, N.; Wu, Y. Investigation on wind tunnel tests of the Kilometer skyscraper. *Eng. Struct.* **2017**, *148*, 340–356. [CrossRef]
32. Clancy, L.J. *Aerodynamics*; Pitman Publishing: London, UK, 1978.
33. Munson, B.R.; Okiishi, T.H.; Rothmayer, A.P.; Huebsch, W.W. *Fundamentals of Fluid Mechanics*; John Wiley & Sons: Hoboken, NJ, USA, 2014.
34. Okuda, Y.; Tanike, Y. On the flow and pressure field around a three dimensional prism (Part 2). *Disaster Prev. Res. Inst. Annu. B* **1990**, *33*, 297–308.
35. Geurts, C.P.W. *Wind-Induced Pressure Fluctuations on Building Facades*; Technische Universiteit Eindhoven: Eindhoven, The Netherlands, 1997.
36. Mendis, P.; Ngo, T.; Haritos, N.; Hira, A.; Samali, B.; Cheung, J. Wind loading on tall buildings. *Electron. J. Struct. Eng.* **2007**, *7*, 41–54.
37. Jamil, M.; Parsa, S.; Majidi, M. Wind Power Statistics and an Evaluation of Wind Energy Density. *Renew. Energy* **1995**, *6*, 623–628. [CrossRef]
38. Yildiz, F. Potential Ambient Energy-Harvesting Sources and Techniques. *J. Technol. Stud.* **2009**, *35*, 40–48. [CrossRef]
39. Elvin, N.G.; Elvin, A.A. An experimentally validated electromagnetic energy harvester. *J. Sound Vib.* **2011**, *330*, 2314–2324. [CrossRef]
40. Hendijanizadeh, M.; Sharkh, S.M.; Elliott, S.J.; Moshrefi-Torbati, M. Output power and efficiency of electromagnetic energy harvesting systems with constrained range of motion. *Smart Mater. Struct.* **2013**, *22*, 125009. [CrossRef]